JUNE, 1976 MATT-1259

NONLINEAR SATURATION OF THE DISSIPATIVE TRAPPED-ION MODE BY MODE COUPLING

BY

BRUCE I. COHEN, JOHN A. KROMMES
W. M. TANG AND MARSHALL N. ROSENBLUTH

PLASMA PHYSICS LABORATORY

PRINCETON UNIVERSITY
PRINCETON, NEW JERSEY

This work was supported by U. S. Energy Research and Development Administration Contract E(11-1)-3073. Reproduction, translation, publication, use and disposal, in whole or in part, by or for the United States Government is permitted.

DISCLAIMER

NOTICE

Printed in the United States of America.

Available from
National Technical Information Service
U. S. Department of Commerce
5285 Port Royal Road
Springfield, Virginia 22151
Price: Printed Copy $ * ; Microfiche $1.45

*Pages	NTIS Selling Price
1-50	$ 4.00
51-150	5.45
151-325	7.60
326-500	10.60
501-1000	13.60

Nonlinear Saturation of the Dissipative Trapped-Ion Mode by Mode Coupling

Bruce I. Cohen, John A. Krommes,†
W.M. Tang, and Marshall N. Rosenbluth†
Plasma Physics Laboratory, Princeton University
Princeton, New Jersey 08540

ABSTRACT

The nonlinear saturation of the dissipative trapped-ion mode is analyzed. The basic mechanism considered is the process whereby energy in long wavelength unstable modes is nonlinearly coupled via $\underset{\sim}{E} \times \underset{\sim}{B}$ convection to short wavelength modes stabilized by Landau damping due to both circulating and trapped ions. In the usual limit of the mode frequency small relative to the effective electron collision frequency, a one-dimensional nonlinear partial differential equation for the potential can be derived, as first shown by LaQuey, Mahajan, Tang, and Rutherford. The stability and accessibility of the possible equilibria for this equation are examined in detail, both analytically and numerically. The equilibrium emphasized by LaQuey et al. is shown to be unstable. However, a class of nonlinear saturated states which are stable to linear perturbations is found. Included in the analysis are the effects of both ion collisions and dispersion due to finite ion banana-width effects. Cross-field transport is estimated and the scaling of the results is considered for tokamak parameters (specifically those for the Princeton Large Torus). It is concluded that the anomalous cross-field transport can be much lower than the estimate of Kadomtsev and Pogutse, for relevant parameters.

1. INTRODUCTION

It is well known that microinstabilities involving magnetically trapped particles [1-10] represent a potentially serious threat to efficient plasma confinement in toroidal systems. Experiments now in operation, such as the Princeton Large Torus (PLT), are expected to reach ion temperatures high enough so that both electrons and ions will have orbits in the "banana" regime, defined by $\omega_{Bi}/\nu_+ > 1$, where ω_{Bi} is the trapped-ion bounce frequency for oscillations between magnetic mirrors and ν_+ is the effective ion collision frequency. Under these conditions it is predicted that unstable drift waves, called dissipative trapped-ion modes, will be generated. The threat of anomalously large transport [11,12] due to this instability has motivated detailed theoretical study of its linear [1-8] and, to a lesser extent, its nonlinear [9,10,13] properties. The purpose of this paper is to consider mode-coupling mechanisms for saturation, in much more breadth and detail than previously [10].

The dissipative trapped-ion mode is a low frequency, electrostatic drift wave propagating in the electron diamagnetic direction. The wave is destabilized by electron collisions and stabilized by ion collisional damping [1,4] and Landau damping due to both circulating [3,4] and trapped [5] ions. Ellipticity of the torus [5], toroidal gradient drifts [7], and impurity density gradients in the direction of the electron and primary ion species density gradients [8] have been demonstrated to be stabilizing. Most of the theoretical treatments cited have been carried out in the radially local limit. The basic assumption

here is that radial excursions of the trapped particles are negligible; i.e. the mode is localized in a region small relative to the plasma radius but large relative to the banana width. The linear radial problem has been studied by Gladd and Ross [6], who found that magnetic shear exerts an additional stabilizing influence. Since shear is not a key ingredient of the coupling mechanism we discuss, we use the local approximation for simplicity. We will only consider the coupling of flute-like modes at radii where the modes have appreciable amplitude, viz. between mode rational surfaces [4,6].

Since proposed operating parameters of PLT, T - 10, and future generation tokamaks fall in the regime where the trapped-ion instability is theoretically predicted to appear, understanding the nonlinear saturation and the concomitant anomalous transport is very important. However, comparatively little research has been done on the nonlinear saturation [9,10,13]. The γ/k^2 estimate of the diffusion coefficient, first proposed by Kadomtsev and Pogutse [11], is widely accepted as an upper limit (γ is the linear growth rate of the fastest growing mode with wavenumber k). The physical arguments of Kadomtsev and Pogutse are based on quasilinear estimates of the level of turbulence necessary to give rise to sufficient diffusive loss (provided by turbulent $\underset{\sim}{E} \times \underset{\sim}{B}$ convection) to effect net stabilization [12]. Jablon proposed that electrostatic detrapping of marginally trapped ions can nonlinearly saturate the instability at a fluctuation level low enough to give substantially less transport than the Kadomtsev-Pogutse estimate [9]. LaQuey,

Mahajan, Rutherford and Tang (LMRT)[10] considered a slab model first proposed by Kadomtsev and Pogutse [11,12], and demonstrated that the instability can be saturated by the nonlinear $\underset{\sim}{E} \times \underset{\sim}{B}$ coupling of energy from unstable long-wavelength modes to short-wavelength modes which are stabilized by ion Landau damping for sufficiently weak temperature gradients: $\eta_i \equiv d \ln(T_i)/d \ln(n_o) < 2/3$. LMRT found coherent, saturated states composed of many Fourier modes, on the basis of which they estimated particle transport. However, the stability or accessibility of those equilibria was not investigated. Ehst has given a general survey of some of the saturation mechanisms for the trapped-ion mode [13].

In this paper we reconsider and extend the model of LMRT. We begin with the field-line averaged continuity, momentum, and quasineutrality equations, introduce slab coordinates, treat collisions with a Krook model, and include in an ad hoc but reasonable fashion the important kinetic effects of ion Landau damping [3-5] and finite ion banana-width effects. Then, following LMRT, we construct a relatively simple model nonlinear equation for the electrostatic potential [Eq. (7)]. The linearized equation gives the correct linear dispersion relation (with the omission of more complicated linear effects such as toroidal gradient drifts, noncircular cross-sections, and impurities). The correct dependence of the linear dispersion relation on the effective ion collision frequency has been lost because of the crudeness of the collision operator [4]. However, most of the

essential linear features of the mode are reproduced accurately by our model. Its simplicity permits us to find analytic solutions of the time-dependent equation which describe the nonlinear evolution of the instability for special cases and also analytic solutions describing various saturated states.

We have made a detailed study of the steady-state solutions of the model equation. In particular, we consider the stability and accessibility of various equilibria. Accessibility is determined by constructing both analytic and numerical time-dependent solutions which trace the growth of the instability from thermal level to its eventual saturation. Several analytic techniques are employed in studying the stability of equilibria. The conclusions are in excellent agreement with the numerically observed behavior. The influences of ion collisions and dispersion due to finite ion banana-width on the saturation are also analyzed. Ion collisions are found to uniformly lower all linear growth rates but not to fundamentally alter the nonlinear saturation. Dispersion is found to be unimportant in particular regimes of experimental interest.

The paper is organized as follows. In Section 2 the detailed development of the model equations describing the nonlinear evolution of the mode is reviewed. The nonlinear saturated states found by LMRT are discussed in Section 3, and their stability and accessibility are investigated. In Section 4 important effects due to ion collisions and dispersion are considered. The level of anomalous cross-field transport is calculated in Section 5 and compared with the estimate of

Kadomtsev and Pogutse. This section also contains a discussion of the scaling of our results for general tokamak parameters. Finally, the results and conclusions of our analysis are briefly summarized in Section 6.

2. Formulation of the Model Equations

In this section we motivate and justify the use of the slab model and fluid equations first proposed by Kadomtsev and Pogutse [11,12]. Basically, this involves a four-fluid model consisting of circulating and trapped ions and electrons. Continuity and momentum equations are employed with the high frequency bounce motion of the trapped particles averaged over, and a Krook collision operator is used. Closure is effected by invoking quasi-neutrality, appropriate for this long wavelength, low frequency electrostatic mode. The kinetic effects of ion Landau damping and finite ion banana-width are then incorporated.

The trapped-ion mode is supported by the magnetically trapped ions and electrons whose unperturbed densities are given approximately by $n_{e,i}^T \sim \varepsilon^{1/2} n_o$, where n_o is the equilibrium total number density and $\varepsilon = r/R$ is the inverse aspect ratio. Since small-angle collisions are particularly effective in scattering trapped particles into the loss cone $v_\parallel > \varepsilon^{1/2} v_\perp$, the effective collision frequencies are enhanced and defined by $\nu_- \equiv \nu_e^{eff} = \nu_e/\varepsilon$ and $\nu_+ \equiv \nu_i^{eff} = \nu_i/\varepsilon$ [12]. The mode frequency ω_o is much less than both the trapped-ion bounce frequency ω_{Bi} and the effective electron collision frequency ν_- , but is much

larger than the effective ion collision frequency ν_+. In fact, the mode frequency is so low that it is much smaller than the product of the parallel wavenumber with either the electron or ion thermal velocity. As a consequence, the circulating particles respond adiabatically to potential fluctuations. The trapped particle densities tend to collisionally relax to Boltzmann distributions $n^T_{e,i} \sim \varepsilon^{1/2} n_o \exp(\pm e\phi/T)$. Following Kadomtsev and Pogutse [12], we postulate two dimensional fluid equations for the trapped particle fluid densities $n^T_{e,i}$ and velocities $V^T_{\sim e,i}$, and for the electrostatic potential. These equations describe the quasineutrality condition and the conservation of particles and momentum in the limit of taking the averages in time over the bounce motion and in space along a field line.

The continuity equations are for $T_e = T_i \equiv T$

$$\partial n^T_{e,i}/\partial t + \underset{\sim}{\nabla}\cdot\left(n^T_{e,i}\, V^T_{\sim e,i}\right) = -\nu_{-,+}\left[n^T_{e,i} - \varepsilon^{1/2} n_o \exp\left(\pm e\phi/T\right)\right] . \tag{1}$$

The right-hand side of Eq. (1) describes the collisional relaxation of the trapped particle densities to the values they would acquire if ϕ varied at a rate slow compared to both effective collision frequencies. In the present case where $\nu_- >> \partial/\partial t \sim \omega_o$, this relaxation model predicts that, to lowest order in $|e\phi/T|$ and $|\omega_o/\nu_-|$, the trapped-electron density is given by $n^T_e \approx \varepsilon^{1/2} n_o \exp(e\phi/T)$. The ions have a small effective collision frequency $\nu_+ << \omega_o$; nevertheless, the trapped ions also tend toward a Boltzmann equilibrium but at a rate slow compared to the mode frequency. The trapped-ion density is therefore

determined by the simultaneous solution of the equations for the fluctuating potential and the moments of the electron and ion distribution functions. In writing Eq. (1), we have made a particular choice of gauge: $\int d^3\underset{\sim}{x}\ \phi(\underset{\sim}{x}) = 0$.

The momentum equation satisfied by all four fluid species is

$$n_j m_j \left(\partial_t + \underset{\sim}{V}_j \cdot \underset{\sim}{\nabla}\right)\underset{\sim}{V}_j = n_j q_j \left(-\underset{\sim}{\nabla}\phi + \underset{\sim}{V}_j \times \underset{\sim}{B} c^{-1}\right) - \underset{\sim}{\nabla}\cdot\underset{\approx}{P}_j + n_j m_j \sum_i \nu_{ji}\left(\underset{\sim}{V}_j - \underset{\sim}{V}_i\right) , \tag{2}$$

where j denotes the species, $\underset{\approx}{P}_j$ is the pressure tensor, q_j is the charge, n_j is the number density, and ν_{ji} is the relative collision frequency. As a result of a spatial average along the field-line and the neglect of shear, the magnetic field in Eq. (2) is uniform. For the sake of simplicity we assume that the plasma is isothermal, and omit temperature perturbations.

Because the mode frequency is so low, $\omega_o << k_\parallel (T/m_i)^{1/2}$, $k_\parallel (T/m_e)^{1/2}$, electron and ion free-streaming parallel to $\underset{\sim}{B}$ ensure that the number densities for the circulating ions and electrons are given to good approximation by their quasi-steady equilibrium values $(1 - \varepsilon^{1/2}) n_o \exp(\pm e\phi/T)$ respectively. (Ions have been taken to be singly charged.) Closure is effected by the quasineutrality condition:

$$n_e^T + \left(1-\varepsilon^{1/2}\right) n_o \exp\left(e\phi/T\right) = n_i^T + \left(1-\varepsilon^{1/2}\right) n_o \exp\left(-e\phi/T\right) . \tag{3}$$

We solve Eqs. (1), (2), and (3) perturbatively, expanding the dependent variables in power series expansions in ϕ. We use the usual slab coordinates $x = r$ and $y = r(\theta - \zeta/q)$, where ζ and θ are the toroidal and poloidal angles and q is the safety factor or inverse rotational transform $2\pi/\iota$. The magnetic field is in the z direction, and the density gradient is along x and assumed to be constant (Fig. 1). The pressure is taken to be isotropic perpendicular to the magnetic field, which permits the replacement $\underset{\sim}{\nabla}\cdot\underset{\approx}{P}_j \rightarrow \underset{\sim}{\nabla} p_j \equiv \underset{\sim}{\nabla}(n_j T)$ since $\partial/\partial z = 0$ identically.

In constructing the fluid velocities to second order, we use the ordering $\nu_+ << \omega_o << \nu_-, \omega_{Bi} << \Omega_{e,i}$, where $\Omega_{e,i}$ are the cyclotron frequencies. We determine from Eq. (2) that the lowest order velocities are the diamagnetic drifts: $\underset{\sim}{V}_j^{(o)} \approx \hat{y} cT/q_j B r_n$ where $r_n \equiv |d\ \ell n(n_o)/dx|^{-1}$. We note that $\underset{\sim}{V}_j^{(o)} \cdot \underset{\sim\sim}{\nabla} \underset{\sim}{V}_j^{(o)} = 0$ and point out that our model omits gradient and curvature drifts, which modify the linear theory [7] and could therefore also influence the nonlinear analysis. The first order, perturbed volocities are

$$\underset{\sim}{V}_j^{(1)} \approx c\hat{z} \times \left[\underset{\sim}{\nabla}\phi + \left(\underset{\sim}{\nabla} p_j / n_j q_j\right)^{(1)}\right] B^{-1}$$

$$- \left(q_j/m_j\Omega_j^2\right)\left(\partial_t + \underset{\sim}{V}_j^{(o)} \cdot \underset{\sim}{\nabla}\right)\left[\underset{\sim}{\nabla}\phi + \left(\underset{\sim}{\nabla} p_j / n_j q_j\right)^{(1)}\right] \qquad (4)$$

The second term on the right-hand side of Eq. (4) is an effective polarization drift and is smaller than the first term by $O(\omega_o/\Omega_j)$. The relative fluid drift velocities are no larger than

the order of the largest fluid velocity at each order in the perturbation expansion. Therefore, collisional drag has very little influence on $\underset{\sim}{V}_j^{(1)}$ for $\nu_{+,-} << \Omega_{i,e}$, and to good approximation $\underset{\sim}{V}_j^{(1)} \approx c\hat{z}\times[\underset{\sim}{\nabla}\phi+(\underset{\sim}{\nabla}p_j/n_jq_j)^{(1)}]B^{-1}$. To next order the momentum equation gives

$$0 \approx -\underset{\sim}{V}_j^{(1)}\cdot\underset{\sim\sim}{\nabla}\underset{\sim}{V}_j^{(1)} - \left[\left(n_jm_j\right)^{-1}\underset{\sim}{\nabla}p_j\right]^{(2)} + \left(q_j/m_jc\right)\underset{\sim}{V}_j^{(2)}\times\underset{\sim}{B} ,$$

whose solution is

$$\underset{\sim}{V}_j^{(2)} \approx \left(c/q_jB\right)\hat{z}\times\left[m_j\underset{\sim}{V}_j^{(1)}\cdot\underset{\sim\sim}{\nabla}\underset{\sim}{V}_j^{(1)} + \left(n_j^{-1}\underset{\sim}{\nabla}p_j\right)^{(2)}\right] . \qquad (5)$$

The polarization drifts and collisional drag have been again neglected in the limits $\omega_o << \Omega_j$ and $\nu_j << \Omega_j$. These results can now be used in solving Eq. (1) to second order in the perturbed quantities.

As a consequence of the slab geometry, the contributions to the fluid velocities due to pressure gradients do not lead to a divergence of the flux, i.e.
$\underset{\sim}{\nabla}\cdot[n_jc\hat{z}\times(n_jq_j)^{-1}\underset{\sim}{\nabla}p_j]B^{-1} = (c/q_jB)\underset{\sim}{\nabla}\cdot(\hat{z}\times\underset{\sim}{\nabla}p_j) = 0$ identically, to all orders in ϕ. We assume that the mode has radial structure of characteristic length equal to the spacing between mode rational surfaces [6]; then k_xr_n is large compared to unity but much smaller than ν_-/ω_o or Ω_i/ω_o for PLT parameters (see Section 5). In these limits one can use Eqs. (4) and (5) to demonstrate that the nonlinearity in the continuity equation

arising from the divergence of the flux due to the ponderomotive force $m_j \underset{\sim}{V}_j^{(1)} \cdot \underset{\sim\sim}{\nabla} \underset{\sim}{V}_j^{(1)}$ is smaller than the dominant nonlinear terms arising from $\underset{\sim}{\nabla} \cdot [n_j^{(1)} \underset{\sim}{V}_j^{(1)}]$ by $O[(k_x r_n)^2 |k_y V_* / \Omega_j|] << 1$, where $V_* \equiv -(\varepsilon^{1/2})\ (cT/eB)\ [\partial \ln(n_o)/\partial x]$ is the trapped electron diamagnetic drift velocity. The dominant terms coming from the divergence of the flux in the continuity equations thus arise from the $c\underset{\sim}{B} \times \underset{\sim}{\nabla} \phi / B^2$ drift velocity. Correct to second order, the continuity equation now becomes

$$\partial n_{e,i}^T / \partial t + c\left(\hat{z} \times \underset{\sim}{\nabla} \phi / B\right) \cdot \underset{\sim}{\nabla} n_{e,i}^T = -\nu_{-,+} \left[n_{e,i}^T - \varepsilon^{1/2} n_o \exp\left(\pm e\phi / T\right) \right] . \tag{6}$$

Eqs. (3) and (6) are the model equations proposed by LMRT [10]. With the orderings $\nu_- >> \partial/\partial t \sim k_y V_* >> \nu_+$ and $|e\phi/T| << 1$, it then follows that the fluctuating potential $\Phi \equiv e\phi/T$ satisfies the nonlinear partial differential equation

$$\frac{\partial \Phi}{\partial t} + V_* \frac{\partial \Phi}{\partial y} + \frac{V_*^2}{\nu_-} \frac{\partial^2 \Phi}{\partial y^2} + \frac{V_*}{\varepsilon^{1/2}} \frac{\partial \Phi^2}{\partial y} + \nu_+ \Phi = 0 \tag{7}$$

Nonlinear contributions to Eq. (7) from radial (x) derivatives of Φ are smaller by $(k_x r_n) k_y V_* / \nu_-$ than the nonlinear term retained. These neglected nonlinear terms are still larger than those due to the ponderomotive force by $(k_x r_n)^{-1} \Omega_i / \nu_- \gtrsim 10$ for $k_x \approx \pi k_y$ (see Ref. 6) and expected PLT parameters ($n_o = 10^{14}$ cm^{-3}, $\varepsilon = 1/4$, $B = 50$ kG, $T = 1$ keV and $m_i/m_e = 3600$). They have been included in a preliminary two dimensional study [14].

Linearization of Eq. (7) followed by Fourier analysis yields a linear dispersion relation for the dissipative trapped-ion mode in the fluid limit: $\omega = \omega_R + i(\omega_R^2/\nu_- - \nu_+)$, where $\omega_R \equiv k_y V_*$. The mode is unstable for $\omega_R^2 > \nu_-\nu_+$. As the mode amplitudes grow, long wavelength modes nonlinearly couple to shorter wavelength modes with larger linear growth rates, resulting in increased steepening as $t \to \infty$. As discussed in Ref. 10, Eq. (7) suggests that there is a transfer of wave energy from long to short wavelengths; but without additional physics there is no mechanism for saturation.

At this point, we appeal to the linear kinetic theory of this mode for important effects omitted in the fluid description. We incorporate two kinetic phenomena which play a crucial role in saturating the instability: Landau damping from circulating and trapped ion resonances [3-5], and finite ion banana-width excursions [6,12]. For sufficiently weak temperature gradients, the mode is now stabilized at short wavelengths by Landau damping.

Finite banana excursions lead to small dispersive corrections to the mode frequency. The saturated mode amplitudes are insensitive to dispersion unless dispersion produces frequency mismatches in the coupling of the linear unstable modes comparable to the characteristic linear growth rates ω_R^2/ν_- . The effect of dispersion is reactive, however: although it causes the mode amplitudes to saturate at higher levels, it does not fundamentally alter the physics of the saturation mechanism. A quantitative discussion of the influence of dispersion appears in Section 4.

It is convenient to transform to the frame moving with the trapped-electron diamagnetic drift velocity: $\eta \equiv y - V_* t$. Next, we follow Ref. 10 and include the effect of Landau damping by circulating ions [4] and by trapped-ion bounce resonances[5]:

$$\gamma_{LD} = A' \left(1 - 3\eta_i/2\right) k_y^4 V_*^4 / \omega_{Bi}^3 \ ,$$

where A' is a numerical factor and $\eta_i \equiv d \ln(T_i)/d \ln(n_o) < 2/3$ to ensure damping.

In describing the effect of Landau damping, we have restricted the structure of the model parallel to $\underset{\sim}{B}$ to be that which admits the largest linear growth rates, i.e. the most flute-like mode. For purposes of a radially <u>local</u> treatment, this amounts to assuming $k_{\parallel} = (\ell q - m)/qR \approx 1/2qR$ in evaluating the Landau damping by the circulating ions. However, because the structure along the field line [4,6,7,9] is taken to have a considerable constant component $f(\theta) \approx (1 + \cos\theta)$, the nonlinear coupling of the modes does not vanish upon taking the bounce average. We emphasize that the detailed rigorous development of these considerations is outside the scope of the simple, two-dimensional Kadomtsev-Pogutse fluid equations.

Including Landau damping, Eq. (7) in nondimensional form is

$$\frac{\partial \psi}{\partial \tau} + \frac{\partial^2 \psi}{\partial \xi^2} + \alpha \frac{\partial^4 \psi}{\partial \xi^4} + \nu \psi + \frac{\partial \psi^2}{\partial \xi} = 0 \ , \qquad (8)$$

where $\tau \equiv \omega_o^2 t/\nu_-$, $\xi \equiv \eta/r$, $\psi \equiv (\nu_-/\varepsilon^{1/2}\omega_o)\Phi$, $\omega_o \equiv V_*/r$, and $\nu \equiv \nu_-\nu_+/\omega_o^2$. We have also defined $\alpha \equiv A'(1 - 3\eta_i/2)(\omega_o/\omega_{Bi})^2\nu_-/\omega_{Bi}$, which measures the strength of Landau damping relative to the destabilizing electron collision term. Poloidal periodicity over the length $2\pi r$ requires that solutions of Eq. (8) satisfy boundary conditions $\psi(\xi) = \psi(\xi + 2\pi)$. The terms $\partial\psi/\partial\tau + \partial\psi^2/\partial\xi$ lead to steepening and wave breaking in the absence of stabilizing terms. The electron collisional term $\partial^2\psi/\partial\xi^2$ destabilizes shorter wavelength modes preferentially and therefore aggravates wave steepening. Ion collisions $\nu\psi$ are unable to stabilize short wavelength modes, and Landau damping $\alpha\partial^4\psi/\partial\xi^4$ is required to effect overall saturation.

We consider both analytic and numerical solutions of Eq. (8) in the following sections. As an introduction, we outline here the types of numerical runs which were performed and the principal conclusions drawn from them. Appendix 1 contains a brief discusssion of the numerical method employed for integrating Eq. (8). The integrations have been performed for both odd parity modes (Fourier sine series) and mixed parity solutions, both with and without collisions, and for a wide range of physically reasonable α (Sec. 3). We have also integrated the extension of Eq. (8) to include a dispersive term $\delta\partial^3\psi/\partial\xi^3$ (Sec. 4). As initial conditions we used either low level noise (constant amplitude times random phase) in all the Fourier components or analytically predicted equilibria

possibly with small perturbations superimposed. For fixed α, many of the runs were performed with both kinds of initial conditions. If a final state can be reached from random noise, then that state is accessible; the evolution of perturbed analytic equilibria yields information about the stability of those equilibria.

In the long time, nonlinear regime of Eq. (8), we observe two qualitatively distinct types of behavior: either time-independent states in which only one linearly unstable mode and its stable first harmonic are significantly excited ("two-mode equilibria"), or time varying but bounded states whose spectral components appear to shift periodically between several adjacent two-mode states whose fundamental is near the fastest growing linearly unstable mode. We describe these time-varying states as "bouncy." Which state is actually observed depends on the value of α in a way which we can predict analytically (Sec. 3).

The analytic equilibrium stressed by LMRT [10] is never observed as the final state, even when inserted as an initial condition. This implies instability of that equilibrium and is an important conclusion of this work; we verify this result analytically (Sec. 3). These results are insensitive to the presence of ion collisions (Sec. 4). They also persist qualitatively in the dispersive limit, although saturation occurs at higher amplitudes in that case (Sec. 4). We comment further on the details of the numerical experiments in what follows.

3. Saturated States: Dispersionless and Collisionless ($\nu_+ \to 0$) Limit

The simplest saturated states of the trapped ion mode occur when effects due to dispersion and ion collisions are negligible. In this Section we construct solutions of Eq. (8) in the limit $\nu \to 0$ and review the two basic steady-state solutions ($\partial/\partial t \to 0$) discussed in Ref. 10. We then extend the study of Eq. (8) by examining the stability of the nonlinear equilibria and the time development of the mode toward a stable equilibrium or away from an unstable equilibrium. Assuming that the instability grows from low level random noise, we address the question of accessibility by directly integrating Eq. (8) with a small emission term present. For a few simple cases, we can construct time-dependent analytic solutions of Eq. (8). More generally, we integrate Eq. (8) by numerical means.

The periodic boundary conditions allow the Fourier representation $\psi(\xi,\tau) = \sum_n [a_n(\tau)\sin(n\xi) + s_n(\tau)\cos(n\xi)]$. This general form admits the possibility of mixed parity solutions, i.e. partly anti-symmetric ($a_n \neq 0$) and partly symmetric ($s_n \neq 0$) solutions about $\xi = 0$. Eq. (8) is evidently of odd parity since changing the signs of ξ and ψ leaves the equation invariant. Thus the odd parity modes $a_n(\tau)\sin(n\xi)$ couple only to themselves. However, in mixed parity wave packets there is coupling of even and odd parity modes to one another. This allows the possibility of steady-state solutions with finite group velocity. Substitution of the Fourier expansion into Eq. (8) gives

$$\partial s_n/\partial\tau - \gamma_n s_n = n\sum_m \left(s_{m+n}a_m - s_m a_{m+n} - s_m a_{n-m} \right) \tag{9a}$$

$$\partial a_n/\partial\tau - \gamma_n a_n = \left(n/2\right)\sum_m \left(s_m s_{n-m} + 2s_m s_{m+n} + 2a_m a_{m+n} - a_m a_{n-m} \right), \tag{9b}$$

where $\gamma_n = n^2 - \alpha n^4 - \nu$ and the mode amplitudes are taken to vanish identically for non-positive index: $s_n \equiv a_n \equiv 0$ for $n \leq 0$.

3.1 "Two-Mode" Equilibrium

We first consider solutions where linearly unstable modes a_p, s_p are stabilized by coupling to their damped harmonics a_{2p}, s_{2p} . This situation can arise in two ways. For $\nu = 0$, α is the only free parameter. When $1/4 < \alpha < 1$ only the $p = 1$ modes are unstable. The quadratic nonlinearity then couples the stable $p = 2$ harmonics to the $p = 1$ modes; a balance of energy flow can be achieved, assuring saturation. In fact, a similar process can occur even when many modes are unstable. For $0 < \alpha < 1/4$ the relative mode spacing around the most unstable modes, $p \approx (2\alpha)^{-1/2}$, is given by $p^{-1} \approx (2\alpha)^{1/2}$ which may <u>not</u> be infinitesimal for typical tokamak parameters (Sec. 5). Then, if the linearly unstable modes are assumed to grow from a small initial level, the most unstable modes will soon acquire a much larger amplitude than their neighbors, i.e. mode selection occurs. The harmonics of the most unstable modes, $2p \approx (2/\alpha)^{1/2}$ are stable and will be nonlinearly excited to higher levels than their stable neighbors, saturating the growth of the most

unstable modes. Thus, because of the mode selection, "two-mode" equilibria can also arise for systems far from marginal stability: $0 < \alpha < 1/4$. Of course, in such saturated states the higher harmonics 3p,4p,...are also excited. Their amplitudes are small however, relative to the dominant p and 2p modes.

The most general equilibrium composed of modes p and 2p must allow for the possibility of a group velocity u: $\psi(\xi,\tau) = \psi(\xi - u\tau)$, which using Eq. (8) with $\nu = 0$ gives

$$-u\frac{\partial\psi}{\partial\xi} + \frac{\partial^2\psi}{\partial\xi^2} + \alpha\frac{\partial^4\psi}{\partial\xi^4} + \frac{\partial\psi^2}{\partial\xi} = 0 \ . \tag{10}$$

The coupled mode equations derived from Eq. (9) then become

$$-pu\begin{bmatrix} a_p \\ -s_p \end{bmatrix} - \gamma_p\begin{bmatrix} s_p \\ a_p \end{bmatrix} = p\begin{bmatrix} s_p a_{2p} + s_{2p} a_p \\ s_p s_{2p} + a_p a_{2p} \end{bmatrix},$$

$$-2pu\begin{bmatrix} a_{2p} \\ -s_{2p} \end{bmatrix} - \gamma_{2p}\begin{bmatrix} s_{2p} \\ a_{2p} \end{bmatrix} = p\begin{bmatrix} 2s_p a_p \\ s_p^2 - a_p^2 \end{bmatrix} \ . \tag{11}$$

In the drifting frame the origin of coordinates can be chosen so that $s_p \equiv 0$. Then solving Eqs. (11), one obtains $a_{2p} = -\gamma_p/p$, $s_{2p} = -u$, $a_p^2 = -\gamma_p\gamma_{2p}/p^2 + 2u^2$, and $-(2\gamma_p + \gamma_{2p})u = 0$. For $2\gamma_p + \gamma_{2p} \neq 0$ the drift velocity u

must vanish, and the equilibrium is described by

$$a_p = \pm\left(-\gamma_p\gamma_{2p}\right)^{1/2}/p \ , \ a_{2p} = -\gamma_p/p \ , \ s_p = s_{2p} = 0 \ . \qquad (12)$$

For $2\gamma_p + \gamma_{2p} = 0$ ($\alpha p^2 = 1/3$) the drift velocity u is indeterminate, and the truncation of the higher harmonics becomes suspect. However, the solutions Eq. (12) for $u = 0$ are allowed, correspond to minimum total energy $E = (1/2)\sum_m m^2(a_m^2+s_m^2) = (1/2)\gamma_p|\gamma_{2p}| + 2\gamma_p^2$, and are in fact observed as the final state in the direct numerical integrations of Eq. (8) whenever time-independent states exist. A steepened wave form typical of this class of equilibria is shown in Fig. 2.

As stated earlier, the numerical integrations reveal that time-independent states do not exist for some values of α. This suggests that the two-mode states are unstable for these α . We now verify this analytically. The linear stability theory of the basic two-mode equilibria is straightforward. From (9b), the mode coupling equation for odd parity solutions can be written

$$\partial a_\ell/\partial\tau = \gamma_\ell a_\ell - (1/2)\,\ell\sum_{\ell'=-\infty}^{\infty} a_{\ell-\ell'}a_{\ell'} \ ,$$

where $a_{-\ell} \equiv -a_\ell$. Linear perturbations δa_ℓ then satisfy

$$\partial\delta a_m/\partial\tau = \gamma_m\delta a_m - m\sum_{\ell=-\infty}^{\infty} a_\ell\delta a_{m-\ell} \ . \qquad (13)$$

The replacement $\partial/\partial\tau \to -i\omega$ yields the eigenvalue equation.

We choose a two-mode equilibrium with fundamental mode number $\ell = L$. It is convenient to scale L from the problem by dividing Eq. (13) by L^3: $\hat{a}_p \equiv a_p/L$, $\delta\hat{a}_p \equiv \delta a_p/L$, $\hat{\omega} \equiv \omega/L^2$, $\hat{\gamma}_p \equiv \gamma_p/L^2$, and $\epsilon \equiv m/L$. We also define $f \equiv \alpha L^2$. The characteristic equation then becomes

$$\det\left(i\hat{\omega}\ \underset{\approx}{I} + \underset{\approx}{D}\right) = 0 \ , \tag{14}$$

where $I_{ij} \equiv \delta_{ij}$ and $D_{ij}(\epsilon,f) = \hat{\gamma}_{\epsilon+(N+1-i)}\delta_{ij} - [\epsilon+(N+1-i)]\hat{a}_{j-i}$, and we retain in the equilibrium the amplitudes $a_{nL}, n=1,2,\ldots,N$. For a particular f, solutions of (14) for ω which lie in the lower half-plane for all ϵ are stable. The heavily damped nature of the high harmonics allows one to truncate the matrix in Eq. (14) at a finite, reasonably small order.

The only calculation which is analytically tractable corresponds to the case with perturbed mode amplitudes (δa_m , δa_{L-m} , δa_{L+m}). However, for $m/L \ll 1$ these modes are all linearly unstable. There is no stable eigenvalue in this case; couplings to the damped modes $\delta a_{2L\pm m}$, etc., must be included in the analysis, which must now be treated numerically.

For the numerical computations to determine the stability of two-mode equilibria, we have found it adequate to choose N = 4 [we compute the equilibrium amplitudes a_{3L} , a_{4L} perturbatively using the values (12)]. By taking proper account of the symmetries of (14), we can then deal with the truncated 5 × 5 matrix describing the system composed of δa_m , $\delta a_{L\pm m}$, $\delta a_{2L\pm m}$.

The results are displayed in Fig. 3. The abscissa describes the possible fundamental mode numbers L of the equilibria; the ordinate describes the Landau damping parameter α . Stable ranges of α for integral L are shown by the vertical solid lines. Since these regions do not overlap for the values of L shown on the graph, certain α's are always unstable. Very roughly, the stable range of α is given by $0.6 < \alpha L^2 < 0.7$. This is in agreement with the numerical results. For values of α which fall outside the predicted stability window, time-dependent "bouncy" states are observed. In these bouncy states, mode configurations are observed to wander or bounce from one grossly perturbed two-mode equilibrium to another after a period of rapid linear growth. For these cases the time-averaged total energy for the final state is observed to scale as $E = (1/4 \pm 1/8)\alpha^{-2}$ for moderate α.

When an α is chosen which is predicted to be stable for a characteristic mode number L, it is generally observed that the numerical solutions actually achieve that time-independent two-mode equilibrium, given sufficient time. For example, the LMRT parameter $\alpha = 0.01$ corresponds to a stable $L = 8$ configuration, which is observed numerically. For $\alpha \lesssim 10^{-3}$ there can be more than one two-mode equilibrium falling within the stability window $0.6 \lesssim \alpha L^2 \lesssim 0.7$. Numerical integration has verified the stability of the equilibrium determined by $\alpha = 10^{-3}$ and $L = 25$ when subject to linear perturbation.

Fig. 2 illustrates the evolution of a twenty mode system of odd parity with $\alpha = 0.05$, initially in an $L = 3$, two-mode equilibrium. According to Fig. 3, there is no stable two-mode equilibrium possible for this system.

Fig. 2 illustrates the growth of m = 1 and m = 2 perturbations leading to a new equilibrium. An examination of the Fourier amplitudes of the final state reveals that all modes are excited, but preferentially those even indexed modes of long wavelength. The scaling of the total energy, which for the two-mode equilibria with $\nu = 0$ and $L = 1/(2\alpha)^{1/2}$ (corresponding to the most unstable mode) is given by $E = (1/2)\gamma_L |\gamma_{2L}| + 2\gamma_L^2 = 3/8\alpha^2$, is still proportional to α^{-2} with a numerical factor of O(1/4).

It should be noted that the predictions of stable equilibria are valid only in the limit of very long time. In certain cases where modes were excited from steady low level emission of random noise, the system of modes did not in fact settle into steady configuration even when stable equilibria were predicted: apparently "bouncy" states were obtained here as well. We believe that in these cases the numerical integrations have perhaps not been carried long enough. Clearly, the time spent in wandering or bouncing before settling on a stable configuration is sensitive to initial conditions. Its scaling with α is uncertain because the characteristic linear growth rates scale as α^{-1}, but the density of two-mode equilibria scales as $\alpha^{-1/2}$ which exerts an opposite influence as α is changed. If the system approaches close enough to a stable two-mode equilibrium, then the mode configuration snaps into and remains in that stable steady state.

To understand in some detail how the modes develop linearly in time and eventually saturate by harmonic generation, we analytically integrate Eqs. (9) for the case of two odd parity Fourier modes:

$$\partial a_L/\partial\tau - \gamma_L a_L = La_L a_{2L} \ , \quad \partial a_{2L}/\partial\tau - \gamma_{2L} a_{2L} = -La_L^2 \ . \tag{15}$$

For $(2\alpha)^{-1/2} < L < \alpha^{-1/2}$ and $\nu \to 0$, we have $4 < |\gamma_{2L}/2\gamma_L| < \infty$; we are thus motivated to make the approximation $|\partial a_{2L}/\partial\tau| \sim |2\gamma_L a_{2L}| << |\gamma_{2L} a_{2L}|$. The harmonic is then driven by the fundamental $a_{2L} \approx La_L^2/\gamma_{2L}$, and Eqs. (15) can be immediately integrated to give

$$a_{2L}(\tau) \approx La_L^2(\tau)/\gamma_{2L} \approx \frac{[La_L^2(0)/\gamma_{2L}]\exp(2\gamma_L\tau)}{1-L^2a_L^2(0)(\gamma_L|\gamma_{2L}|)^{-1}[1-\exp(2\gamma_L\tau)]} \tag{16}$$

Thus a_L grows exponentially at rate γ_L and excites its harmonic at rate $2\gamma_L$. The growth of both modes is essentially exponential in time until the last e-folding when the nonlinearity in Eq. (15) for a_L is finally of sufficient magnitude to saturate growth.

In a similar manner, Appendix 2 considers the more complicated mode structure composed of unstable odd parity modes with indices m,ℓ, and ℓ+m and heavily damped modes 2ℓ-m , 2ℓ, 2ℓ+m, 2ℓ+2m, and 2ℓ+3m. This system is shown to have no steady-state with a_m,a_ℓ, and $a_{\ell+m}$ all finite. With $a_m = 0$ the familiar two-mode equilibrium (a_ℓ,$a_{2\ell}$) or ($a_{\ell+m}$,$a_{2\ell+2m}$) can be achieved. For $a_m \neq 0$ the "bouncy" behavior, which characterizes the nonlinear oscillations of the mode amplitudes observed at effective saturation in some of the numerical integrations, is mimicked in a simple fashion.

3.2 LMRT Equilibrium

In this section we discuss a second class of equilibria of Eq. (8), originally derived and emphasized by LMRT [10]. These multi-mode equilibria consist of a rapid spatial variation with wavenumber near marginal stability $k_y \sim 1/\alpha^{1/2}r$, modulating factors to satisfy the periodic boundary conditions, and couplings to the harmonics $n/\alpha^{1/2}r$, $n = 2,3,...$ LMRT believed these equilibria to be the only ones relevant for situations far from marginal stability ($\alpha << 1$), the regime of most physical interest. Transport estimated on this basis is generally optimistic, i.e. it is smaller than that computed from the two-mode equilibria [10] and generally smaller than the Kadomtsev-Pogutse estimate.

However, there are important deficiencies in the LMRT treatment. The magnitude of the transport depends on a parameter m, $0 \leq m < 1$, extremely sensitive to small changes in α . For $m \to 1$ the transport diverges and the ordering assumed by LMRT is violated. LMRT estimated transport by considering the largest m for which the fundamental orderings were expected to hold. In view of the near divergence, however, this procedure is both dangerous and somewhat arbitrary. Furthermore, LMRT did not address the important questions of stability and accessibility of the equilibria.

In fact, we demonstrate both analytically and numerically that the LMRT equilibria are always unstable. Therefore, such states are not expected to be observed experimentally. We further prove that both the two-mode equilibria and the LMRT

states emerge from a complete multiple space scale analysis of Eq. (8) for small α . In fact, for a critical value of $f \equiv \alpha\ell^2 = f_c \equiv 1 - 1/12\ell^2$, the LMRT state coalesces with a two-mode equilibrium composed of modes varying as $\sin(\ell\xi)$ and $\sin(2\ell\xi)$.

A review of the LMRT equilibrium construction and a discussion of the coalescence with the two-mode equilibrium are presented in Appendix 3. Here, we formulate and solve the problem of the stability of the LMRT equilibria. We follow LMRT in making the multiple space-scale decomposition

$$\psi(\xi,\tau) = A(\xi,\tau) + \mathrm{Im}[C(\xi,\tau)\exp(i\ell\xi)] + \mathrm{Im}[C_2(\xi,\tau)\exp(i2\ell\xi)], \quad (17)$$

where A is real, C and C_2 are generally complex, and A, C, and C_2 are slowly varying relative to $\exp(i\ell\xi)$: $|\partial \ln A/\partial\xi| = O(1) << \ell$, etc. We insert Eq. (17) into Eq. (8) with $\nu \to o$ and equate the coefficients of $1, \exp(i\ell\xi)$, and $\exp(i2\ell\xi)$ to obtain three coupled nonlinear equations for A, C, and C_2:

$$\partial A/\partial\tau + \left(\partial/\partial\xi\right)\left(A' + A^2 + |C|^2/2 + |C_2|^2/2\right) = 0 , \quad (18a)$$

$$\left(\partial/\partial\tau\right)(C/2i) + \left(\partial/\partial\xi + i\ell\right)\left[-i\left(AC - \lambda C'\right) + \ell\hat{\gamma}_\ell C/2 + 3fC''/2\ell + C^*C_2/2\right] = 0 , \quad (18b)$$

$$\left(\partial/\partial\tau\right)\left(C_2/2i\right) + \left(\partial/\partial\xi + 2i\ell\right)\left\{\left[2AC_2 + \left(1 - 12f\right)C_2'\right]/2i + \left(\ell\hat{\gamma}_{2\ell}C_2 + 12fC_2''/\ell\right)/4\right\} = 0, \quad (18c)$$

where primes denote derivatives with respect to ξ . In writing (18c) Eq. (18) we have neglected C''' and defined $\lambda \equiv (3f - 1)/2$. For the remainder of this section it will be adequate to take $\lambda = 1$ (see Appendix 3). We assume that $\partial/\partial\tau = O(1)$ and $\hat{\gamma}_{2\ell} = O(1)$ (for f sufficiently far from 1/4). It is then clear from (18c) that to dominant order in $1/\ell$

$$c_2 = c^2/\ell\hat{\gamma}_{2\ell} \cdot \tag{19}$$

We thus neglect the last term in (18a). Expressions for the equilibrium ($\partial/\partial\tau \equiv 0$) quantities A and C are given in Appendix 3.

In the linear stability analysis we examine only those perturbations retaining the form of (17); we ignore possible decays into waveforms of different fundamental wavenumber $\ell' \neq \ell$. This is sufficient since even this restricted configuration is always unstable. Perturbing (18b) and using (19) yields

$$0 = \left(\partial/\partial\tau\right)\left(\delta C/2i\right) + \left(\partial/\partial\xi + i\ell\right)\left\{-i\left(A\delta C + C\delta A - \delta C'\right) + \ell\hat{\gamma}_\ell \delta C/2 + 3f\delta C''/2\ell + \left[2|C|^2 \mathrm{Re}\left(\delta C/C\right)C + |C|^2\delta C\right]/2\ell\hat{\gamma}_{2\ell}\right\} . \tag{20}$$

It is convenient to define $\delta D \equiv \delta C/C \equiv \delta\rho + i\delta\phi$; upon inserting this into (20) and using the equilibrium equations, we find that many terms proportional to δD vanish. Ordering in $1/\ell$, separating real and imaginary parts, and replacing $\partial/\partial\tau \to -i\omega$, we find finally that

$$-i\omega\delta A + (\partial/\partial\xi)(\delta A' + 2A\delta A + |C|^2\delta\rho) = 0 \ , \tag{21a}$$

$$\delta A = \delta\rho' \ , \tag{21b}$$

$$-i\omega\delta\rho/2 - \ell[-\delta\phi' + 3(\delta\rho'' + 2\rho'\delta\rho')/2\ell + |C|^2\delta\rho/\ell\hat{\gamma}_{2\ell}] = 0, \tag{21c}$$

where $\rho' \equiv \mathrm{Re}(C'/C)$. We insert (21b) into (21a) and integrate to obtain

$$L_\omega\delta\rho \equiv \left[\frac{d^2}{d\xi^2} + 2A\frac{d}{d\xi} + |C|^2 - i\omega\right]\delta\rho = \mu(\omega) \ , \tag{22a}$$

$$\delta\rho'(0) = \delta\rho'(\pi) = 0 \ , \tag{22b}$$

where μ is an integration constant. We impose periodicity on ϕ and average (21c) over 0 to π :

$$0 = i\omega\langle\delta\rho\rangle/2 + 3\langle A\delta\rho'\rangle + \hat{\gamma}_{2\ell}^{-1}\langle|C|^2\delta\rho\rangle \ . \tag{23}$$

Integrating the second term by parts using the equilibrium boundary condition $A(0) = A(\pi) = 0$, we can rewrite (23) as

$$0 = F\{\delta\rho\} \equiv \langle(i\omega/2 - 3A' + \hat{\gamma}_{2\ell}^{-1}|C|^2)\delta\rho\rangle \ , \tag{24}$$

where F is a linear functional of its argument. Eqs. (22) and (24) constitute a linear eigenvalue problem, somewhat complicated by the spatial dependence of the equilibrium.

One case, however, can be treated exactly, and yields useful insight. Namely, at the coalescence point for the LMRT and two-mode equilibria, we show in Appendix 3 that $A \equiv 0$ and $C \equiv 1$, so that (22) simplifies to

$$\delta\rho'' + \Omega^2\delta\rho = \mu \ , \tag{25}$$

where $\Omega^2(\omega) = 1 - i\omega$. Eq. (24) becomes

$$\left(i\omega/2 + 1/\ddot{\gamma}_{2\ell}\right) \langle\delta\rho\rangle = 0 \ . \tag{26}$$

One possible eigenvalue emerges immediately from (26): $\omega = 2i/\hat{\gamma}_{2\ell}$, which is purely damped since $\hat{\gamma}_{2\ell} < 0$. The general solution of (25) is $\delta\rho = A\cos(\Omega\xi) + \mu/\Omega^2$, where A is a constant. This satisfies the boundary condition $\delta\rho'(0) = 0$. Satisfying the boundary condition at $\xi=\pi$ leads to the eigenvalue condition $\delta\rho'(\pi) = 0 = -\Omega A \sin(\Omega\pi)$, which implies $\Omega=n$, where $n = \pm1, \pm2, \ldots,$ or $\omega=i(n^2-1)$. There is evidently instability for $|n| > 1$. Our orderings break down for $|n| \gtrsim \ell$, but the presence of unstable roots within a circle of radius $O(\ell)$ demonstrates the instability of this particular equilibrium.

The presence of multiple unstable eigenvalues suggests that the entire class of LMRT equilibria $0 < m < 1$ (see Appendix 3) is unstable, since the equilibrium is smoothly varying and the eigenvalues should thus be smooth functions of m. However, it might happen that as $m\to1$ the eigenvalues could move into regimes of the complex plane where our orderings are questionable.

We therefore examine the general case as well.

It is convenient to use a Nyquist technique. We note that for arbitrary ω the boundary value problem Eq. (22) will have in general no nontrivial solution, since unless ω is an eigenvalue we cannot satisfy all of the boundary conditions simultaneously. However, consider the modified problem formed by inserting an impulsive source on the right-hand side of (22):

$$L_\omega \delta\rho = \mu(\omega) + D(\omega)\,\delta(\xi-\xi_o), \quad (0 < \xi_o < \pi)$$

where D is to be determined. Continuity is imposed on $\delta\rho$ at ξ_o: $[\delta\rho]_{\xi_o} = 0$; and $\delta\rho$ is given an arbitrary normalization: $\delta\rho(0) = 1$, which is allowed because the perturbation is linear. We retain the original conditions $F\{\delta\rho\} = 0$, $\delta\rho'(0) = \delta\rho'(\pi) = 0$. We then have five conditions to be imposed on the solution $\delta\rho$ of an inhomogeneous, linear, second-order differential equation, with one unknown constant μ, in two adjacent domains. Therefore, a nontrivial solution exists to this new problem for all complex ω; this solution <u>determines</u> D as $D(\omega) = [\delta\rho']_{\xi_o}$. Furthermore, since D vanishes identically when ω is an eigenvalue, $D(\omega) = 0$ is an effective dispersion relation. This function can thus be plotted in the usual way as a function of the Nyquist contour in Fig. 4a. If D encircles the origin, an unstable root lies within the contour (assuming no poles are enclosed as well). These ideas can be formulated in a form quite suitable for numerical analysis by using a Green's function technique (Appendix 4).

In general the dispersion function D may have poles as well as zeros. This is illustrated in Appendix 4 by the form of D for the coalesced equilibrium. Since the Nyquist method actually provides only the difference in the number of zeros and poles encircled, the Nyquist plot may not encircle the origin even though the contour encloses an unstable eigenvalue. This problem is easily dealt with by deforming the Nyquist contour (Fig. 5a).

In Fig. 4b we show the topology of the numerically computed Nyquist plot for m = 0.15 and the contour of Fig. 4a with nondimensional radius equal to five. The plot encircles the origin, indicating instability. For m = 0.23 the modified contour in Fig. 5a is deformed around the poles of $D(\omega)$ and indicates an unstable eigenvalue (Fig. 5b). Proceeding in this way, we can in fact demonstrate that all the LMRT equilibria are unstable with eigenvalues $|\omega| \approx O(1)$, which are within the limits of validity of the theory.

We have verified these analytic predictions by numerical experiments. The LMRT equilibria are never observed when the partial differential equation (8) is integrated in time with random noise as initial condition. Furthermore, we have employed the LMRT equilibria as initial values, perturbed these equilibria slightly, and examined their subsequent evolution in time. In every case, the equilibria decay immediately, either into time-independent two-mode equilibria or into "bouncy" saturated states. Fig. 6 shows the results of a computer experiment portraying the evolution of a perturbed

coalesced equilibrium. Appearing in Fig. 7 are the results of a computer experiment following the decay of a perturbed LMRT wave form using parameters close to those for the wave form displayed in Fig. 1 of Ref. 10. There is an increase in the total field energy in both cases, and the peaks of the energy spectra move to longer wavelength, closer to the most unstable modes.

4. Dispersion and Ion Collisions

In this section we expand our discussion of the saturation of the trapped-ion mode to include additional linear effects, namely the dispersion produced by finite ion banana excursions and the dissipation due to ion collisions. Since the saturation mechanism investigated in this paper relies on nonlinear processes mediating a balance between opposing linear effects destabilizing and stabilizing the modes, additional linear features of the mode may have a strong influence on the nonlinear saturation. We demonstrate that dispersion does not fundamentally alter the saturation mechanism. It does, however, provide an effective impedance which can inhibit mode coupling and result in saturation at significantly higher mode amplitudes for sufficient dispersion [15]. We also find that, aside from uniformly decreasing the growth rates of the unstable modes and further stabilizing the damped modes, ion collisions do not significantly affect the nonlinear saturation of systems far from marginal stability ($\alpha << 1$).

4.1 Dispersive Effects

For $T_e \approx T_i \equiv T$ important dispersive effects arise from the delocalization due to the finite ion banana-width. The periodic component of the average effective delocalization length perpendicular to the field line is given by the ion banana-width $\rho_i q/\varepsilon^{1/2}$, where ρ_i is the ion gyro-radius [16]. In the limit $\omega << \omega_{Bi}$, the linear dispersion relation including the ion banana-width correction, but omitting Landau damping, is given by [6]

$$\frac{2}{\varepsilon^{1/2}} = \frac{\omega-\omega_*}{\omega+i\nu_-} + \frac{\omega+\omega_*}{\omega+i\nu_+}\left(1-b\right) , \qquad (27)$$

where $\omega_* = -k_y(cT/eB)[\partial \ln(n_o)/\partial x]$ is the electron diamagnetic drift frequency and $b \approx (k_x^2 + k_y^2)\rho_i^2 q^2 \varepsilon^{-1} << 1$. In obtaining Eq. (27), we have assumed that the bounce motion and therefore the periodic component of the ion banana excursions have an approximately harmonic time dependence, which with the usual Bessel function identity and subsequent expansion for small argument b gives a correction of characteristic form (1-b) in the term arising from the trapped-ion response.

The real part of the frequency becomes $\mathrm{Re}(\omega) \approx \varepsilon^{1/2}\omega_*(1-b)/2$. If the linear, radial structure of all the modes corresponds to the lowest mode found by Gladd and Ross [6], then the frequency shift $\Delta\omega \approx -\varepsilon^{1/2}\omega_* k_x^2 \rho_i^2 q^2/2\varepsilon$ can be absorbed by a further change of reference frame and the radial mode structure otherwise ignored, provided we consider only the <u>local</u> nonlinear evolution

far from radial nodes. Detailed consideration of radial effects is deferred to a future study. Dispersion is then modeled in the radially local, one dimensional approximation by adding to Eq. (8) the term $\delta\partial^3\psi/\partial\xi^3$, where $\delta \equiv (\nu_-/\omega_o)(\rho_i^2 q^2/\epsilon r^2)$ measures the approximate relative level of dispersion:

$$\frac{\partial\psi}{\partial\tau} + \frac{\partial^2\psi}{\partial\xi^2} + \alpha\frac{\partial^4\psi}{\partial\xi^4} + \nu\psi + \delta\frac{\partial^3\psi}{\partial\xi^3} + \frac{\partial\psi^2}{\partial\xi} = 0 \ . \qquad (28)$$

We expect the influence of dispersion to become significant when the nonlinear three-wave interactions of the unstable modes (index $m < \alpha^{-1/2}$) with the linearly damped modes ($m > \alpha^{-1/2}$) acquire frequency mismatches comparable in size to the characteristic rates of the three-wave interactions. From Eqs. (15) and (16), these rates are of order twice the linear growth rates of the unstable modes. For $\nu \to 0$ this is equivalent to balancing the $\partial^2\psi/\partial\xi^2$ term with the $\delta\partial^3\psi/\partial\xi^3$ term in Eq. (28) for $|\partial/\partial\xi| \sim m \sim \alpha^{-1/2}$. We conclude that dispersion will have a significant influence on the saturation for $\delta/\alpha^{1/2} \gtrsim 1$. We evaluate this condition for expected PLT tokamak parameters and typical plasma profiles in the next section.

Dispersive corrections from the real part of the dielectric response of the barely trapped and circulating ions, the imaginary part of whose response gives the Landau damping, can also be important. However, because of the dependence on $k_\parallel$ and thus on shear, we defer detailed study of these effects to a future publication. We proceed on the basis that inclusion of these and other dispersive corrections only modifies the radially local parameter dependence of δ.

In the dispersive limit, two-mode equilibria with a finite group velocity u are possible. We use Eq. (28) with $\nu \to 0$ and rewrite Eqs. (10) and (11) to obtain the steady-state, coupled-mode equations:

$$-\left(\delta p^2 + u\right) p a_p = p s_{2p} a_p \ , \ -\gamma_p a_p = p a_p a_{2p}$$

$$-2p\left(4\delta p^2 + u\right) p a_{2p} - \gamma_{2p} s_{2p} = 0 \ , \ 2p\left(4\delta p^2 + u\right) s_{2p} - \gamma_{2p} a_{2p} = - p a_p^2 p \ , \tag{29}$$

where we have again set $s_p = 0$. Eqs. (29) are readily solved to give

$$a_{2p} = -\gamma_p / p \ , \ s_{2p} = -\left(\delta p^2 + u\right), \text{ and } a_p^2 = -\gamma_{2p}\gamma_p^{-1}\left(\delta p^2 + u\right)^2 - \gamma_{2p}\gamma_p / p^2 \ , \tag{30a}$$

and

$$u = -\delta p^2 \left(8\gamma_p + \gamma_{2p}\right) / \left(\gamma_{2p} + 2\gamma_p\right) = 2\delta p^2 \left(1 - 2\alpha p^2\right) / \left(3\alpha p^2 - 1\right) \tag{30b}$$

As $\delta \to 0$, these solutions join smoothly onto the earlier two-mode equilibrium configurations Eqs. (12). The total energy of the drifting steady state is larger than for the nondispersive case:

$$E = p^2 a_p^2 / 2 \ + \ 2p^2\left(a_{2p}^2 + s_{2p}^2\right) = |\gamma_{2p}|\gamma_p / 2 + 2\gamma_p^2 + \beta\delta^2 p^6 \ , \tag{31}$$

where $\beta \equiv 36\left(2 - \gamma_{2p}/2\gamma_p\right)\gamma_p^2 / \left(\gamma_{2p} + 2\gamma_p\right)^2 > 0$. The first two terms on the right-hand side of Eq. (31) scale as p^4. Therefore the last term, which represents the additional saturation

energy due to dispersion, scales relative to the sum of the first two terms as $\delta^2 p^2 = \delta^2/\alpha$ for $p = O(\alpha^{-1/2})$. Then, in agreement with our earlier estimate, the influence of dispersion is appreciable when $\delta/\alpha^{1/2} \gtrsim O(1)$.

We remark that for modes such that $\gamma_{2p} + 2\gamma_p \to 0$ ($\alpha_p^2 \approx 1/3$), u and the amplitudes a_p and s_{2p} apparently diverge. In this limit it is invalid to truncate the higher harmonics 3p,4p,... In general, dispersive equilibria are expected to have amplitudes and group velocities as continous functions of α . In any case, nonlinear saturation evidently occurs at a higher level than in the absence of dispersion. Relatively large amplitude equilibria can be achieved which are consistent with our theory provided that the group velocity remains small, i.e. $|\omega_o^2 ur/\nu_-| << V_*$, and provided $|e\phi/T| \approx |\omega_o \varepsilon^{1/2} \psi/\nu_-| << 1$. In the limit $|u| >> \delta p^2$, the latter condition becomes $|e\phi/T| = O|\omega_o \varepsilon^{1/2} u/\nu_-| << 1$. When the equilibria are highly dispersive, incoherent processes [9,13], which are complementary to the resonant mode-coupling considered here, are presumed to play more of a role in the saturation.

Direct numerical integrations of Eq. (28) confirm that again the two-mode equilibria achieved by harmonic generation are the relevant mode configurations. Eqs. (30) describe the steady states obtained when the modes are excited by steady random emission at low level and when judicious choice of α is made so that $|1-3\alpha p^2|$ is finite. The arguments pertaining to Eq. (16) made earlier (Sec. 3) describe in spirit the accessibility of the two-mode states with finite dispersion. The main

difference is that dispersion steadily mixes phase and imposes a reactive load on the mode coupling.

4.2 Ion Collisions

The principal effect of ion collisions is to uniformly reduce the linear growth rates, $\mathrm{Im}(\omega) = k_y^2 v_*^2/\nu_- - \gamma_{LD} - \nu_+$ or nondimensionally $\gamma_m = m^2 - \alpha m^4 - \nu$ (see Fig. 8). If the effective ion collision frequency is sufficiently high ($\nu > 1/2\alpha$), the trapped-ion instability is suppressed altogether. Thus for instability, ion temperatures will have to be high enough so that $\nu_+ << \omega_{Bi}$ and $\nu_+ < \omega_o^2/4\alpha\nu_-$. These considerations based on the linear theory help to define the relevant plasma conditions for the mode and serve as starting point for our examination of its nonlinear saturation.

Fig. 8 illustrates how ion collisions could subtly alter nonlinear stabilization by mode coupling. In the absence of collisions, mode coupling effectively transfers wave energy from unstable longer wavelength modes to an energy sink at shorter wavelengths provided by Landau damping. If $\nu > 1$, ion collisions can supply an additional energy sink at long wavelength, which is accessible by three-wave decay of the linearly unstable waves. We examine a new class of equilibria made possible by the energy sink at long wavelength, but we determine that they are not accessible and are unstable.

A simple analytic treatment can be given which is appropriate for systems with finite rather than infinitesimal

α, where $\alpha < 1$. In the nondispersive limit we hypothesize steady-state solutions of Eq. (8) composed of three odd parity Fourier modes (p,2p,3p), since the ion collision term does not mix parity. The coupled-mode equations obtained from Eq. (9),

$$\partial a_p/\partial\tau - \gamma_p a_p = p a_p a_{2p} + p a_{2p} a_{3p} ,$$

$$\partial a_{2p}/\partial\tau - \gamma_{2p} a_{2p} = -p a_p^2 + 2_p a_p a_{3p} , \tag{32}$$

$$\partial a_{3p}/\partial\tau - \gamma_{3p} a_{3p} = -3_p a_p a_{2p} ,$$

have steady solutions ($\partial/\partial\tau \equiv 0$), which are most simply given in the limit $|\gamma_p/\gamma_{3p}| << 1$ by

$$a_p = \pm\left(-\gamma_p\gamma_{2p}\right)^{1/2}/p \ , \ a_{2p} = -\gamma_p/p, \text{and } a_{3p} = \pm\left(3\gamma_p/p\gamma_{3p}\right)\left(-\gamma_p\gamma_{2p}\right)^{1/2} \tag{33a}$$

or

$$a_p = \pm\left(-\gamma_{2p}\gamma_{3p}/3p^2\right)^{1/2} , \ a_{2p} = -\gamma_{3p}/3_p \ , \text{ and } a_{3p} = \pm\left(-\gamma_{2p}\gamma_{3p}/3p^2\right)^{1/2} \tag{33b}$$

The validity of Eqs. (33a) [Eqs. (33b)] requires that $-\gamma_p\gamma_{2p} > 0$ [$-\gamma_p\gamma_{2p} < 0$] and that the mode amplitude a_{4p} is so heavily damped that it can be neglected.

The solutions described by Eqs. (33a) are the same as the two-mode equilibria described by Eq. (12), the finite amplitude

of a_{3p} serving as a small correction. However, we now realize that these steady-state solutions generally apply for $\gamma_p \gtrless 0$ provided that $-\gamma_p\gamma_{2p} > 0$. The set of solutions Eqs. (33b) can arise for $\gamma_{2p} \gtrless 0$ if $-\gamma_{2p}\gamma_{3p} > 0$. Eqs. (32), or Eq. (8) more generally, will govern the time development of the mode amplitudes excited from low levels initially and will determine the accessibility of a steady state.

We investigate the accessibility of the three-mode configuration in which $\gamma_{3p} << \gamma_p < 0$ and $-\gamma_{3p} >> \gamma_{2p} > 0$. To lowest order in $|\gamma_{3p}^{-1}\,\partial/\partial\tau|$, a_{3p} is quasi-steadily driven by the beat $a_p a_{2p}$. Eqs. (32) can be expressed in the form

$$a_{3p} \approx -3_p|\gamma_{3p}|^{-1}\, a_p a_{2p} \tag{34a}$$

$$\partial a_p/\partial\tau \approx \left[p\left(1-3_p|\gamma_{3p}|^{-1}a_{2p}\right)a_{2p} - |\gamma_p|\right] a_p \tag{34b}$$

$$\partial a_{2p}/\partial\tau \approx \left(|\gamma_{2p}| - 6p^2|\gamma_{3p}|^{-1}a_p^2\right)a_{2p} - pa_p^2 \tag{34c}$$

During the linear growth phase $a_{2p} \sim a_{2p}(0)\exp(\gamma_{2p}\tau)$, we observe that for $a_{2p}(0) < 0$ Eq. (34b) describes the exponential <u>decrease</u> of a_p at a rate faster than the exponential increase of a_{2p}. This causes a_{3p} to decrease as well, and no saturation of the growth of a_{2p} is possible unless the stable harmonic a_{4p} is included.

For $a_{2p}(0) > 0$, Eqs. (34b) and (34a) describe the

concomitant growth of modes a_p and a_{3p}, driven by the decay of the exponentially growing mode a_{2p} to a_p and the subsequent beating of a_{2p} with a_p to excite a_{3p}. The amplitudes of the three modes will stabilize at the values given by Eqs. (33) if the right-hand sides of Eqs. (34b) and (34c) can vanish simultaneously. In Eq. (34b) the amplitude a_{2p} determines the growth of a_p. It is evident that if all three modes are excited initially from low level, a_p first <u>decreases</u> in magnitude, since $\partial \ln a_p/\partial\tau < 0$ for $a_{2p} < |\gamma_p| p^{-1}$. For $|\gamma_p| p^{-1} < a_{2p} < |\gamma_{3p}| (3p)^{-1}$, $\partial \ln a_p/\partial\tau > 0$. However, before a_p can sufficiently grow to attain an equilibrium value, a_{2p} overshoots the value $|\gamma_{3p}| (3p)^{-1}$ resulting in $\partial \ln a_p/\partial\tau < 0$ which further destabilizes a_{2p} as described by Eq. (34c). Numerical integrations verify the overshoot and runaway phenomena described here.

We remark that the harmonic generation of the damped mode a_{4p} omitted in Eqs. (32) to (34) proceeds at rate $2\gamma_{2p}$. Thus the excitation of a familiar two-mode equilibrium (2p,4p) occurs on the time scale of the linear exponential growth of the mode a_{2p} when the mode a_{4p} is included; therefore, overshoot and runaway of a_{2p} cannot really occur. Furthermore, we observe that when a system of modes is initially prepared in one of the three-mode states described by Eqs. (33) for γ_p, $\gamma_{3p} < 0$ and $\gamma_{2p} > 0$, the mode configuration is unstable to the formation of a (2p,4p) equilibrium (see Fig. 9).

We have also investigated the influence of ion collisions on the LMRT equilibria. Because the LMRT solutions are composed of weakly damped or weakly growing modes with a particular ordering of parameters, the nondimensional ion collision frequency ν cannot exceed O(1), otherwise there will be no linearly unstable modes. We have extended the LMRT equilibrium solutions to include $\nu = O(1)$ by means similar to those discussed in Section 3, Appendix 3 and Ref. 10. Direct numerical integrations of Eq. (8) with these new equilibrium solutions as initial conditions disclose, however, that ion collisions do not stabilize the LMRT equilibria. The LMRT equilibria are again unstable to the growth of modes with faster linear growth rates (Sec. 3), which subsequently form steady two mode equilibria or time-dependent superpositions of two-mode states.

5. Cross-Field Transport and Scaling for Tokamak Plasmas

5.1 Transport Coefficient for Radial Flux

In this section we consider the enhanced radial transport that arises due to the trapped-ion mode and examine in detail the scaling of our results with physical parameters. In particular, the transport levels for saturation via coherent mode coupling are compared to the transport levels based on turbulent saturation predicted by Kadomtsev and Pogutse [11,12]. We also determine the range of plasma parameters for which our various assumptions are valid, and we calculate the dependence of important dimensionless parameters on the relevant plasma parameters.

The coherent, radial transport is determined locally by the flux $\left\langle n_e^T \underset{\sim}{V}_e^T \cdot \hat{x} \right\rangle$, where the brackets indicate an average over the poloidal angle, i.e. $(2\pi r)^{-1} \int_0^{2\pi r} dy (n_e^T \underset{\sim}{V}_e^T \cdot \hat{x})$. Because of the poloidal periodicity, the contribution to the average flux from the diamagnetic fluid velocity vanishes identically to all orders in $e\phi/T$. The poloidal average is equivalent to a time average over many oscillation periods. The circulating electrons respond adiabatically, and therefore do <u>not</u> give rise to an average radial flux. To lowest order the radial transport is driven by the $\underset{\sim}{E} \times \underset{\sim}{B}$ drift and is given by

$$\left\langle n_e^{T(1)} \underset{\sim}{V}_e^{T(1)} \cdot \hat{x} \right\rangle = (c/B) \left\langle n_e^{T(1)} \hat{z} \times \underset{\sim}{\nabla} \phi \cdot \hat{x} \right\rangle , \qquad (35)$$

and the transport coefficient is

$$D \equiv -\left\langle n_{e\sim e}^{T} V_{\sim}^{T} \cdot \hat{x} \right\rangle / \left(\partial n_o/\partial x\right) \approx \left(c/B\right)\left(\partial n_o/\partial x\right)^{-1} \left\langle n_e^{T(1)} \nabla_y \phi \right\rangle \qquad (36)$$

The contributions to the flux from $n_j^{T(0)} V_{\sim j}^{T(2)}$ induced by the ponderomotive force have been assumed small, an assumption which is justified later in this section.

We construct n_i^T in terms of ϕ from Eqs. (3) and (6) by eliminating n_e^T assuming $|e\phi/T| << 1$ and $\nu_- >> \omega_o >> \nu_+$. It is straightforward to show that $n_e^T = n_i^T - 2n_o\Phi(1-\varepsilon^{1/2})$ and

$$n_i^T \approx \varepsilon^{1/2} n_o + 2\Phi n_o(1 - \varepsilon^{1/2}/2 + \nu_+/\nu_-) - 2n_o(V_*/r\nu_-)\partial\Phi/\partial\xi$$

$$+ 2n_o(V_*/r\varepsilon^{1/2}\nu_-)\partial\Phi^2/\partial\xi + \ldots . \qquad (37)$$

where $\Phi \equiv e\phi/T$.

Substitution of Eq. (37) into (36) yields

$$D \approx \left(\frac{cT}{eB}\right)^2 \frac{\varepsilon^{1/2}}{\nu_-} \left\langle \left(\frac{\partial\Phi}{\partial y}\right)^2 \right\rangle = \frac{\varepsilon^{3/2}}{\nu_-} \left(\frac{\omega_o}{\nu_-}\right)^2 \left(\frac{cT}{reB}\right)^2 \left\langle \left(\frac{\partial\psi}{\partial\xi}\right)^2 \right\rangle , \qquad (38)$$

which agrees with a derivation from quasilinear kinetic theory. The transport coefficient is therefore directly proportional to $\langle(\partial\psi/\partial\xi)^2\rangle = \sum_m m^2(a_m^2+s_m^2)/2$, which is just the nondimensional energy E expressed in terms of the Fourier coefficients introduced preceding Eq. (9). Kadomtsev and Pogutse have suggested a transport coefficient due to incoherent, turbulent

processes which is given by $D_{KP} \sim (r/R)^{5/2}(cT_e/eB)^2/4\nu_e r_n^2$, which we will compare with Eq. (38) in the following.

5.2 Scaling of Results for Tokamak Plasmas

For purposes of application we consider reference parameters typical for PLT operation: $n_o \approx 10^{14}cm^{-3}$, B = 50kG, $\varepsilon_o \equiv \varepsilon(a)=1/3$, $m_i/m_e = 3600$, a = 45cm , R = 135cm, $\eta_i = 1/2$, $q_o \equiv q(0) = 1.25$, and $T_o \equiv T(0) = 1$ keV.

As was defined following Eq. (8), $\alpha = A'(1-3\eta_i/2)(\omega_o/\omega_{Bi})^2\nu_-/\omega_{Bi}^T$. If we use the conventional definition $\omega_{Bi} \equiv \varepsilon^{1/2} V_i/qR$, where V_i is the ion thermal velocity, and refer to the literature for the contributions to Landau damping from the trapped [5] and the circulating [4] ions, we obtain $A' \simeq 40$. We recall that $\omega_o = V_* r^{-1} = \varepsilon^{1/2}\rho_i V_i/4r_n r$. For PLT parameters $\rho_i = 0.13T(keV)^{1/2}B(50kG)^{-1}$ and $\nu_e \approx 4 \times 10^5\, n(10^{14}cm^{-3})T(keV)^{-3/2}$. Hence

$$\alpha \approx 5.5 \times 10^{-4} q^3\, \varepsilon^{-7/2} R r_n^{-2} n\left(10^{14}cm^{-3}\right) B\left(50kG\right)^{-2} T\left(keV\right)^{-1}\left(1-3\eta_i/2\right). \tag{39}$$

To maintain the validity of the fluid treatment, it is required that Im $\omega < k_y V_*$ and consequently that α be not too small, viz. $\alpha^{1/2} > \omega_o/\nu_-$. For typical plasma profiles and parameters α is of order 10^{-3} or 10^{-2} . Similarly , we find that

$$\omega_o/\omega_{Bi} = 3.25 \times 10^{-2} q\varepsilon^{-1} r_n^{-1} T\left(keV\right)^{1/2} B\left(50kG\right)^{-1} \tag{40}$$

and

$$\omega_o/\nu_- = 2.5\ \varepsilon^{3/2}\left(\frac{r}{r_n}\right)^{-1}T\left(\text{keV}\right)^{5/2}n\left(10^{14}\text{cm}^{-3}\right)^{-1}B\left(50\text{kG}\right)^{-1}\ , \qquad (41)$$

both of which have been assumed small.

In Section 2 the model, one-dimensional partial differential equation, Eq. (8), is derived assuming that the ponderomotive nonlinearity is small compared to the neglected terms involving x derivatives coming from $\nabla\cdot[n_j^{(1)}\underset{\sim}{v}_j^{(1)}]$, which in turn are assumed small compared with the retained terms containing the y derivatives from $\nabla\cdot[n_j^{(1)}\underset{\sim}{v}_j^{(1)}]$. The validity of the latter assumption depends on

$$k_x r_n \omega_o/\nu_- << 1\ , \qquad (42)$$

and the former on

$$\Omega_i/\left(k_x r_n \nu_-\right) >> 1\ . \qquad (43)$$

Gladd and Ross [6] have investigated the linear radial mode structure of the trapped-ion mode and have shown that $k_x \sim \pi/\Delta r_s$, where Δr_s is the spacing between mode rational surfaces: $\Delta r_s = (\ell\, dq/dr)^{-1}$, and ℓ is the toroidal mode number. We use $\ell q \approx m \sim O(\alpha^{-1/2})$, where m is the poloidal mode number, and $rd[\ln(q)]/dr = O(1)$ to obtain $k_x r_n \approx O(\pi k_y r_n) \sim r_n/\alpha^{1/2}r$. Excluding the exact center of the cross-section, there is a large fraction of the plasma volume over which $r_n/r = O(1)$. Then

$k_x r_n \sim \pi k_y r_n \sim \pi\alpha^{-1/2} = O(30)T(keV)^{1/2} n(10^{14}cm^{-3})^{-1/2}$ for typical PLT parameters ($\varepsilon \approx 1/4$ and $q \approx 2.5$). We use Eq. (40) and $\Omega_i/\nu_- = 1.2 \times 10^3\ \varepsilon B(50kG)T(keV)^{3/2} n(10^{14}cm^{-3})^{-1}$ to evaluate the inequalities (42) and (43):

$$k_x r_n \omega_o/\nu_- \approx 6 \times 10^{-3} T(keV)^3 n(10^{14}cm^{-3})^{-3/2} << 1 \qquad (44a)$$

and

$$\Omega_i/(k_x r_n \nu_-) \approx 10T(keV)n(10^{14}cm^{-3})^{-1/2} >> 1\ , \qquad (44b)$$

using B = 50kG, $\varepsilon \approx 1/4$, and $q \approx 2.5$. These inequalities are well satisfied for PLT parameters and justify the one-dimensional model.

In our analysis we further assume that $e\phi/T$ is small. In the absence of dispersion we have found that the saturated amplitude scales as $\psi \sim \alpha^{-1/2}$ which gives $e\Phi/T \sim \varepsilon^{1/2}\omega_o/\nu_-\ \alpha^{1/2}$ or

$$e\phi/T \sim 10^2\ \varepsilon^{11/4}\left(1-3\eta_i/2\right)^{-1/2}\ R^{-3/2}q^{-3/2}n\left(10^{14}cm^{-3}\right)^{-3/2}T\left(keV\right)^3. \qquad (45)$$

For parameters typical of the heart of the PLT profile: $\varepsilon \sim 1/4$, $q \sim 2.5$, and $r_n/R \sim 1/3$, Eqs. (39) and (41) give

$$\alpha \approx 0.07(1-3\eta_i/2)n(10^{14}cm^{-3})T(keV)^{-1}$$

and

$$\omega_o/\nu_- \approx 2.1 \times 10^{-4} n(10^{14}cm^{-3})^{-1} T(keV)^{5/2}\ .$$

Then $|e\phi/T|$ being small depends on $\omega_o/\nu_- << 1$, and we find that

$$|e\phi/T| \approx 0.4 \times 10^{-3}(1-3\eta_i/2)^{-1/2} n(10^{14}\text{cm}^{-3})^{-3/2} T(\text{keV})^3 .$$

This level is competitive with the estimates for saturation by means of electrostatic detrapping [9,13]. Because $n\lambda_D^3 \approx 10^6 n(10^{14}\text{cm}^{-3})^{-1/2} T(\text{keV})^{3/2}$, the thermal fluctuation level is small by comparison, viz. $|e\phi/T| \lesssim O(10^{-3}) n(10^{14}\text{cm}^{-3})^{1/4} T(\text{keV})^{-3/4}$. Our numerical studies of Eq. (8) indicate that the saturated amplitudes are insensitive to noise at this relative level.

In order that the trapped-ion mode be linearly unstable, the effective ion collision frequency must not be too large, $\nu_+ < \omega_o^2/2\alpha\nu$. (see Sec. 4). Using $\nu_+ = (m_e/m_i)^{1/2}\nu_-$, $m_i/m_e = 3600$, and Eqs. (39) and (41), we determine that the condition for instability is

$$2\alpha\nu_-\nu_+/\omega_o^2 \approx 3 \times 10^{-6} q^3 R^3 \varepsilon^{-9/2} n\left(10^{14}\text{cm}^{-3}\right)^3 T\left(\text{keV}\right)^{-6} \left(1-3\eta_i/2\right) < 1. \qquad (46)$$

We note that the l.h.s. of (46) is a sharply decreasing function of temperature and inverse aspect ratio and increases dramatically with increasing density.

We recall from Section 4 that the nonlinear saturation is relatively insensitive to dispersion provided that $\delta < \alpha^{1/2}$ and that the quantity $|1-3\alpha p^2|$ is not too small. For intermediate

sized α typical for PLT plasma parameters, e.g. $\alpha = 0.01$, we find that $|3\alpha p^2 - 1| > 0.08$; and therefore the two-mode, drifting equilibrium solutions described by Eqs. (30) are well-behaved. Dispersive effects due to finite ion banana-width will then be of little consequence if

$$\delta/\alpha^{1/2} \approx 0.6\, q^{1/2}\, \varepsilon^{-1/4} r^{1/2} \left(r_n/r\right)^2 n\left(10^{14}\mathrm{cm}^{-3}\right)^{1/2} T\left(\mathrm{keV}\right)^{-1} < 1 \tag{47}$$

We can now remark that evidently the relative influences of dispersion and ion collisions both decrease as the plasma temperature increases, which make those simplest considerations of the mode saturation appearing in Sec. 3 relevant in the high temperature limit. The radial transport in the collisionless and nondispersive limits can be compared to Kadomtsev and Pogutse's D_{KP} by use of Eq. (38):

$$D/D_{KP} \approx 2.1 \times 10^7 r_n^4 \left(\varepsilon/qR\right)^6 \left(1 - 3\eta_i/2\right)^{-2} B\left(50\mathrm{kG}\right)^2 n\left(10^{14}\mathrm{cm}^{-3}\right)^{-4} T\left(\mathrm{keV}\right)^7 \tag{48}$$

We can now summarize the various validity conditions $\omega_o \ll \omega_{Bi}$, $\omega_o \ll \nu_-$, $\nu_+ < \omega_o^2/2\alpha\nu_-$, and $\delta < \alpha^{1/2}$ and the condition that the calculated transport be more optimistic than the Kadomtsev and Pogutse prediction $D < D_{KP}$. We use Eqs. (42), (43), (46), (47), and (48) to determine a set of critical central temperatures as functions of $x \equiv r/a$ where the conditions become equalities. For purposes of illustration we employ PLT parameters and reasonable plasma density and temperature profiles,

$n(x) = n_o(1-x^2)$, $q(x) = q_o(1+x^2)$, and $T(x) = T_o(1-x^2)^{1/2}$: then $r_n = a(1-x^2)/2x$ and $\eta_i = \eta_e = 1/2$. For the given profiles we then obtain

$$\omega_o << \omega_{bi} \gtrless T_o << T_B \equiv 2.4 \times 10^2 \left(\frac{\varepsilon_o aB}{q_o} \right)^2 \frac{(1-x^2)^{3/2}}{(1+x^2)^2} =$$

$$3.4 \times 10^4 \frac{(1-x^2)^{3/2}}{(1+x^2)^2} ,$$

$$|e\phi/T| << 1 \gtrless T_o << T_\phi \equiv 0.17 \left(\frac{R_o q_o n_o}{\varepsilon_o^2} \right)^{1/2} \varepsilon_o^{1/12} \frac{x^{1/12}}{x} (1+x^2)^{1/2} =$$

$$6x^{-11/12} \left(1+x^2\right)^{1/2} ,$$

$$\omega_o << \nu_- \gtrless T_o << T_- \equiv 0.53 \left(\frac{n_o BRa}{\varepsilon_o^{1/2}} \right)^{2/5} \left(\frac{1-x^2}{x^2} \right)^{3/10} =$$

$$21.5x^{-3/5} \left(1-x^2\right)^{3/10} ,$$

(49)

$$\nu_+ < \omega_o^2/2\alpha\nu_- \gtrless T_o > T_+ \equiv 0.08 \left(\frac{n_o q_o R}{\varepsilon_o^{3/2}} \right)^{1/2} x^{-3/4} \left(1+x^2\right)^{1/2} =$$

$$2.36x^{-3/4} \left(1+x^2\right)^{1/2} ,$$

$$\delta < \alpha^{1/2} \gtrless T_o > T_D \equiv 0.144 \, \varepsilon_o^{1/4} \left(Rq_o n_o \right)^{1/2} \frac{x^{1/4}}{x^4} \left(1-x^2\right)^2 \left(1+x^2\right)^{1/2} =$$

$$1.4 \frac{x^{1/4}}{x^4} \left(1+x^2\right)^{1/2} \left(1-x^2\right)^2 ,$$

and

$$D < D_{KP} \rightleftarrows T_o < T_{KP} \equiv 0.10\left(\frac{q_o R}{\varepsilon_o}\right)^{6/7} \frac{n_o^{4/7}}{a^{4/7} B^{2/7}} \frac{(1+x^2)^{6/7}}{x^{2/7}(1-x^2)^{1/2}} =$$

$$2.36 \frac{(1+x^2)^{6/7}}{x^{2/7}(1-x^2)^{1/2}} ,$$

where the density is in units of $10^{14} cm^{-3}$, the magnetic field is in units of 50kG and the temperatures are in keV.

The central temperatures determined by Eqs. (49) are tabulated for three radial locations in Table 1. The column for $T_o < T_B$ has been omitted since the condition $\omega_o << \omega_{bi}$ is easily satisfied everywhere in the profile except at the limiter. Table 1 indicates that the trapped-ion mode will occur throughout a substantial volume of the PLT plasma for central temperatures in excess of 4 or 5 keV. For these temperatures the fluctuating potential will saturate at levels $e\phi/\varepsilon T < O(0.1)$. Dispersive effects seem to be small over a large part of the cross-section, but significant for $x \leq 0.5$. We note here that Table 1 is somewhat misleading on the subject of transport, because the transport coefficient relative to the Kadomtsev-Pogutse estimate Eq. (48) scales very sharply with respect to temperature, $D/D_{KP} \propto T^7$. For example, a central temperature of T_o = 4keV would allow the trapped-ion mode to occur for $x > 0.75$; the saturation would probably be nondispersive, $\delta << \alpha^{1/2} \lesssim O(0.05)$, and result in a relative transport

TABLE 1. CRITICAL CENTRAL TEMPERATURES (KEV) FOR PRINCETON LARGE TORUS PLASMA PARAMETERS AND PROFILES.

x	$T_o << T_\phi$	$T_o << T_-$	$T_o > T_+$	$T_o > T_D$	$T_o < T_{KP}$
.25	25	48	6.9	233	3.8
.5	14	30	4.4	12	4.0
.75	10	20	3.7	1.0	5.7

coefficient $D/D_{KP} \leq (4/5.7)^7 \approx 0.1$. However, for higher central temperatures, D/D_{KP} rapidly increases and other nonlinear effects become important. Because of the requirements $T_o << T_\phi$ and $T_o << T_-$, our basic theoretical model begins to break down in such a temperature range. Note that for larger devices as R increases the range of applicability of the theory also increases.

6. CONCLUSIONS

We have presented a detailed study of the saturation of the dissipative trapped-ion mode by the mode coupling of unstable long-wavelength modes to modes at shorter wavelength stabilized due to Landau damping by trapped and circulating ions. We have found that stable "two-mode" equilibria can be achieved by means of harmonic generation of short wavelength, stable modes. However, the multi-mode steady states emphasized by LaQuey et al are always unstable.

These results were obtained analytically and verified by detailed numerical experiments. In particular, the numerical studies have verified that coherent, two-mode steady states can be excited from steady emission of random noise. Even when there is competition between two or more two-mode configurations in the time-asymptotic state, the effective saturated amplitudes and wave energies scale approximately as a single two-mode equilibrium.

Although ion collisions are important in the linear stability theory of the mode, we have shown that, other than

uniformly decreasing the growth rates of all modes, they do not fundamentally influence the saturation mechanism. With regard to finite ion banana-width dispersive effects, we conclude that dispersion does not alter the basic saturation mechanism. However, it can inhibit mode-coupling and drive the saturated amplitudes to much higher and possibly inaccessible levels, if the dispersion produces a relative frequency shift comparable to the linear growth rates of the most unstable modes. In the dispersive limit, other complementary saturation mechanisms, e.g. electrostatic detrapping and quasilinear profile modification, may dominate.

Finally, we have applied our considerations to expected plasma profiles and parameters for PLT and determined in detail the limits of applicability of our model. Of particular interest, we have calculated the enhanced radial transport due to the trapped-ion mode and have compared it with Kadomtsev and Pogutse's rough estimate. We find that the relative transport is extremely sensitive to temperature, $D/D_{KP} \propto T^7$. For PLT central temperatures high enough to overcome the instability threshold determined by ion collisions and Landau damping for $r > 0.5a$, it is required that $T_o \gtrsim 4$keV; and we find that the relative transport is small: $D \lesssim 0.1 D_{KP}$. For $T_o > 6$keV, $D >> D_{KP}$ and other nonlinear effects can become important. Note, however that with increasing temperature the theoretical model employed begins to break down. We also note that when mode coupling provides the dominant saturation mechanism, the saturated amplitudes and transport levels (for PLT parameters) are competitive with the best estimates of those corresponding to saturation by electrostatic detrapping [13].

ACKNOWLEDGEMENTS

We wish to express our appreciation to P.K. Kaw, C. Oberman, F.W. Perkins, G. Rewoldt, and P.H. Rutherford, for numerous helpful discussions and encouragement.

This work was supported by the U.S. Energy Research and Development Administration Contract Nos. E(11-1)-3073 and E(11-1)-3237.

APPENDIX 1. Numerical Algorithm for Coupled-wave Equations

Our numerical integrations have made use of a computational scheme suggested by F.W. Perkins. The linear variations of the mode amplitudes are analytically absorbed into an integrating factor, leaving the nonlinear variations to be integrated approximately. The latter frequently make more modest demands on the time step for numerical integrations, since they often occur on a time scale lower than the linear variations.

Eqs. (9) can be generalized to include the parity mixing effect of dispersion and written in the symbolic form

$$\partial \underset{\sim}{\psi}/\partial\tau - \underset{\approx}{L}\cdot\underset{\sim}{\psi} = \sum_{\sim} \left(\underset{\sim}{\psi}\right) , \qquad (1.1)$$

where $\underset{\sim}{\psi} \equiv (s_1, s_2, \ldots, a_1, a_2, \ldots)$; $\underset{\approx}{L}$ is a linear tensor operator corresponding to linear growth, dissipation, and dispersion; and $\sum_{\sim} (\underset{\sim}{\psi})$ is the vector corresponding to the nonlinear terms in Eq. (9). The integrating factor or propagator is $\exp(-\underset{\approx}{L}\tau)$ which leads to the result,

$$\underset{\sim}{\psi}\left(\tau+\Delta\tau\right) = \exp\left(\underset{\approx}{L}\Delta\tau\right)\cdot\left[\underset{\sim}{\psi}\left(\tau\right) + \int_0^{\Delta\tau} d\tau' \exp\left(-\underset{\approx}{L}\tau'\right)\cdot\sum_{\sim}\left(\underset{\sim}{\psi}\right)_{\tau+\tau'}\right] . \qquad (1.2)$$

The numerical integration of the nonlinear term on the right-hand side of Eq. (A.2) can then be done by various standard algorithms.

APPENDIX 2. Competition of Two-mode Equilibria

We now consider analytically the time dependence of more complicated mode structures. One multi-mode configuration with some flavor of nondispersive systems far from marginal stability ($\alpha << 1$), but simple enough to permit analytic progress, consists of unstable odd parity modes a_m, a_ℓ, and $a_{\ell+m}$ and heavily damped modes $a_{2\ell-m}$, $a_{2\ell}$, $a_{2\ell+m}$, $a_{2\ell+2m}$, and $a_{2\ell+3m}$. We consider the case where $m << \ell \gtrsim (2\alpha)^{-1/2}$, i.e. the coupling of two unstable modes of nearly maximum linear growth rate to a longer wavelength mode of weaker growth rate. For $|\gamma_{2\ell}/2\gamma_\ell| >> 1$ the damped modes are driven by the unstable, longer wavelength modes, from Eqs. (9)

$$a_{2\ell-m} \approx -\ell\left(2\ell-m\right)\left(\gamma_{2\ell}\gamma_{2\ell-m}\right)^{-1} a_m a_\ell^2 \ , \ a_{2\ell} \approx \ell\gamma_{2\ell}^{-1} a_\ell^2 \ ,$$

$$a_{2\ell+m} \approx \left(2\ell+m\right) \gamma_{2\ell+m}^{-1} a_\ell a_{\ell+m} \ , \ a_{2\ell+2m} \approx \left(\ell+m\right) \gamma_{2\ell+2m}^{-1} a_{\ell+m}^2 \ , \tag{2.1}$$

and

$$a_{2\ell+3m} \approx \left(\ell+m\right)\left(2\ell+3m\right)\left(\gamma_{2\ell+3m}\gamma_{2\ell+2m}\right)^{-1} a_m a_{\ell+m}^2 \ .$$

To good approximation Eqs. (9) also give

$$\partial a_m/\partial\tau - \gamma_m a_m \approx m a_\ell a_{\ell+m} \ ,$$

$$\partial a_\ell/\partial\tau - \gamma_\ell a_\ell \approx \ell a_m a_{\ell+m} + \ell^2\gamma_{2\ell}^{-1} a_\ell^3 + \ell\left(2\ell+m\right) \gamma_{2\ell+m}^{-1} a_{\ell+m}^2 a_\ell \ , \tag{2.2}$$

$$\partial a_{\ell+m}/\partial\tau - \gamma_{\ell+m} a_{\ell+m} \approx -(\ell+m) a_m a_\ell + (\ell+m)^2 \gamma_{2\ell+2m}^{-1} a_{\ell+m}^3 + (\ell+m)(2\ell+m) \gamma_{2\ell+m}^{-1} a_\ell^2 a_{\ell+m} \quad .$$

For $m << \ell$ and $\ell \approx (2\alpha)^{-1/2}$, $\gamma_m/2\gamma_\ell \approx O(m/\ell)^2 << 1$. Therefore a_m is nonlinearly excited by the beat of a_ℓ with $a_{\ell+m}$, and during the early linear growth of the mode amplitudes $a_m \approx m(\gamma_\ell+\gamma_{\ell+m})^{-1} a_\ell a_{\ell+m}$. However, if the system can achieve a steady state, $a_m \approx m\gamma_m^{-1} a_\ell a_{\ell+m}$. It is straightforward to demonstrate that a steady-state solution of Eqs. (2.2) with mode amplitudes a_m , a_ℓ , and $a_{\ell+m}$ all finite requires that $\gamma_{\ell+m} < 0$ in contradiction to the original hypothesis. (Sec. 6 discusses equilibria where γ_m , $\gamma_\ell > 0$ and $\gamma_{\ell+m} < 0$.) If a_m is allowed to vanish, a_ℓ and $a_{\ell+m}$ are uncoupled and the familiar two-mode steady solutions $(a_\ell, a_{2\ell})$ or $(a_{\ell+m}, a_{2\ell+2m})$ can be recovered.

For finite a_m, Eqs. (2.1) and (2.2) describe the time dependence of this multi-mode configuration and imitate in a simplified fashion the behavior of the numerical integrations of Eqs. (9) for $\alpha = O(10^{-2})$ and thirty or more modes. Since $\gamma_{2\ell}$, $\gamma_{2\ell+m}$, $\gamma_{2\ell+2m} < 0$, the growth of modes a_ℓ and $a_{\ell+m}$ is necessarily limited by the nonlinear coupling to damped modes as described in Eqs. (2.2). The difference in signs in the cross-coupling terms $\ell a_m a_{\ell+m}$ and $-(\ell+m) a_m a_\ell$ precludes the continued growth of a_m and is responsible for the nonlinear oscillations of the amplitudes of the linearly unstable modes.

Eqs. (2.1) and (2.2) thus serve as a simple model for the mode competition occuring in the computer studies in which either time-dependent, "bouncy" saturations persist or the configurations seem to snap into steady, two-mode equilibria.

APPENDIX 3. Coalescence of LMRT and Two-Mode Equilibria

We review here the multiple space-scale construction of the LMRT equilibria [10], and discuss their coalescence with the two-mode equilibria. We begin with Eqs. (18a), (18b), and (19) and set $\partial/\partial\tau \equiv 0$ and $C \equiv |C|\exp(i\phi)$ to obtain to dominant order in $1/\ell$

$$A' + A^2 + |C|^2/2 = b/2 \ , \tag{3.1a}$$

$$A = \lambda \ \partial/\partial\xi \ \ln|C| \ , \tag{3.1b}$$

$$\lambda\phi' = \left(1/2\right)\left\{\ell\hat{\gamma}_\ell + \left(1/\ell\right)\left[|C|^2/\hat{\gamma}_{2\ell} + 3f|C|''/|C|\right]\right\} \ , \tag{3.1c}$$

where b is a real integration constant. The appropriate boundary conditions are $A(0) = A(\pi) = 0$ and $\phi(0) = \phi(\pi) = 0$. We have already assumed that $C, C''/C = O(1)$. We then see from (3.1c) that to satisfy the periodic boundary conditions we must have $\hat{\gamma}_\ell = O(1/\ell^2)$, or $f = 1 - O(12\ell^2)^{-1}$. Thus, we can set $f \approx 1$ ($\lambda \approx 1$) everywhere except in $\hat{\gamma}_\ell$ in (3.1c). For notational convenience, we now replace $|C| \to C$. By combining (3.1b) with (3.1a), we find

$$C'' + \left(1/2\right) C\left(C^2-b\right) = 0 \ , \ C'\left(0\right) = C'\left(\pi\right) = 0 \qquad (3.2)$$

Using (3.2) and (3.1c), we can also write

$$\phi' = \left(1/24\ell\right)\left[\left(b_o - C^2\right) + 18\left(b-C^2\right)\right] \ , \qquad (3.3)$$

where $b_o \equiv -\ell\hat{\gamma}_{\ell}\hat{\gamma}_{2\ell} \approx 12\ell(1-f) \equiv a_\ell^2$ is the square of the fundamental amplitude of the two-mode equilibrium corresponding to the given values of f and ℓ. Periodicity is imposed on ϕ in integrating (3.3) from 0 to π:

$$0 = \left(b_o - \langle C^2\rangle\right) + 18\left(b - \langle C^2\rangle\right) \ , \qquad (3.4)$$

where $\langle f(\xi)\rangle \equiv \pi^{-1}\int_o^\pi d\xi f(\xi)$. It is clear that a two-mode equilibrium is indeed a solution of (3.2) and (3.3): $C^2=b_o=b$. Eqs. (3.1b) and (19) provide the remaining information $A = 0$ and $C_2 = -\ell\hat{\gamma}_\ell$.

The LMRT equilibria are defined to be those nontrivial solutions of (3.2) and (3.3) for which $b \neq b_o$. There is a simple interpretation of these which comes from the formal similarity of (3.2) to a particle trapped in a potential well. We can write

$$C'' = -\partial V/\partial C \ , \ V\left(C\right) = \left(1/8\right)C^2\left(C^2 - 2b\right) \ . \qquad (3.5)$$

This potential is sketched in Fig. 10. The boundary conditions in Eq. (3.2) require the "particle" to move across the well in a "time" π (Fig. 10). The two-mode equilibria correspond to the particle being stationary at the bottom of the well.

Eq. (3.5) is readily integrated:

$$\xi/2 = \int_{C_1}^{C} dz \left[\left(C_2^2 - z^2 \right) \left(z^2 - C_1^2 \right) \right]^{-1/2} , \tag{3.6}$$

where $C(0) = C_1$, $C(\pi) = C_2$, and $b = (C_1^2 + C_2^2)/2$. This fixes $C_2 = 2\pi^{-1}K(m)$, where $m = 1 - (C_1/C_2)^2$ and $K(m)$ is the complete elliptic function of the first kind, $0 \leq m < 1$. Then $C_1 = 2\pi^{-1}K(m)(1-m)^{1/2}$, and $b = 4\pi^{-2}K(m)(1-m/2)$. In terms of the Jacobi elliptic function nd, Eq. (3.6) is written

$$C(\xi) = 2\pi^{-1}K(m)\left(1-m\right)^{1/2} \operatorname{nd}\left(\pi^{-1}K(m)\,|\,m\right) . \tag{3.7}$$

This satisfies $\langle C^2 \rangle = 4\pi^{-2}K(m)E(m)$, with $E(m)$ the complete elliptic integral of the second kind. Eq. (3.4) then determines $b(b_o)$, or $m(f,\ell)$. In particular, at $m = 0$ we have $b = C = 1$, and from Eq. (3.4) $b_o = 1$. This is consistent with a two-mode equilibrium for which $f = 1 - 1/12\ell^2$. The domains of existence of the two classes of solutions are illustrated in Fig. 11.

Eqs. (3.1b) and (3.7) provide the result

$$A(\xi) = \pi^{-1}mK(m) \operatorname{nd}\left(\pi^{-1}\xi K|m\right) \operatorname{sn}\left(\pi^{-1}\xi K|m\right)\operatorname{cn}\left(\pi^{-1}\xi K|m\right).$$

In this form, the functional behavior is not transparent. If one combines a small parameter expansion ($m << 1$) of (3.6) with the requirement that the amplitude of C be exactly maintained for all m, one has approximately the simpler forms $C(\xi,m) \approx C_1(m) + \Delta(m)\ \sin^2(\xi/2)$ and $A(\xi,m) \approx (1/2)\ \Delta(m)\sin(\xi)$, where $\Delta(m) \equiv C_2(m) - C_1(m)$. These forms are adequate for a wide range of $m < 1$.

APPENDIX 4. Green's Function Solution for the Dispersion Function $D(\omega)$

We formulate here the solution for the dispersion function $D(\omega)$ in a form suitable for numerical analysis. It is convenient to introduce the Green's function $G(\xi\ ,\ \xi')$ which satisfies the equations

$$L(\xi)\, G(\xi,\xi') = \delta(\xi - \xi') \tag{4.1a}$$

and, with $(\partial/\partial\xi)\, G(\xi\ ,\ \xi') \equiv G'(\xi\ ,\ \xi')$,

$$G'(0,\xi') = G'(\pi\ ,\ \xi') = 0\ , \tag{4.1b}$$

$$\lim_{\varepsilon\to 0} G'(\xi' + \varepsilon,\ \xi') - G'(\xi' - \varepsilon,\ \xi') = 1\ . \tag{4.1c}$$

The solution of (22) with source function added is then

$$\delta\rho = \mu\int_0^{\pi} d\xi'\ G(\xi,\xi') + DG(\xi,\xi_0)\ . \tag{4.2}$$

We define $g(\xi) \equiv G(\xi,\xi_o)$ and $I(\xi) \equiv \int_0^\pi d\xi'\, G(\xi,\xi')$. The normalization $\delta\rho(0) = 1$ allows the replacement of μ using (4.2):

$$\delta\rho = I(\xi)/I(0) + D\left[g(\xi) - I(\xi)\, g(0)/I(0)\right] \tag{4.3}$$

Finally, applying $F\{\delta\rho\} = 0$ from Eq. (24), we obtain $D = F\{I\} / [g(0)F\{I\} - I(0)F\{g\}]$. We recall that the solution of $D(\omega) = 0$ gives the desired dispersion relation describing the stability of the LMRT equilibria.

The auxiliary functions g and I satisfy boundary value problems which are solved by the superposition of the solutions of easily computable initial value problems. In particular, if $L(\bar{g},h,k) = 0$, where $\bar{g}(0) = 1$, $\bar{g}'(0) = 0$, $h(\xi_o) = k'(\xi_o) = 1$, and $h'(\xi_o) = k(\xi_o) = 0$, we have

$$g(\xi) = \Theta(\xi_o - \xi)\, g_<(\xi) + \Theta(\xi - \xi_o)\, g_>(\xi) \ ,$$

with $g_<(\xi) = -k'(\pi)\bar{g}(\xi)/\mathcal{D}$, $g_>(\xi_o) = \bar{g}(\xi_o)[h'(\pi)k(\xi)$

$$- k'(\pi)h(\xi)]/\mathcal{D} \ ,$$

and $\mathcal{D} = \bar{g}'(\xi_o)k'(\pi) + \bar{g}(\xi_o)h'(\pi)$. [$\Theta(\xi)$ is the Heaviside unit-step function.] In similar fashion, if $L\, I_1 = 0$ where $I_1(0) = 1$ and $I_1'(0) = 0$, and if $I_2 = 0$ where $I_2(0) = 0$ and $I_2'(0) = 0$, then we find

$$I(\xi) = [I_1'(\pi)I_2(\xi) - I_2'(\pi)I_1(\xi)]/I_1'(\pi) \ .$$

As an example of these considerations, we find for the uniform, coalesced equilibrium (see Appendix 3)
$D(\omega) = \sin(\Omega\pi)/\{\Omega\cos[\Omega(\pi-\xi_o)] - \sin(\Omega\pi)\}$, where $\Omega^2(\omega) = 1 - i\omega$. We see here explicitly that the dispersion function can have poles as well as zeros, the implications of which in the context of a Nyquist analysis are discussed in the text.

References and Footnotes

†Address: The Institute for Advanced Study, Princeton, New Jersey 08540.

[1] KADOMTSEV, B.B., POGUTSE, O.P., Zh. Eksp. Teo.Fiz. 51, 1734(1966) [Sov. Phys. - JETP 24,1172(1967)]

[2] KADOMTSEV, B.B., POGUTSE, O.P., Dokl.Akad.Nauk SSSR 186, 553(1969) [Sov. Phys. - Dokl. 14,470(1969)].

[3] GALEEV, A.A., SAGDEEV, R.Z., Dokl.Akad.Nauk SSSR 180, 839(1968) [Sov. Phys. - Dokl. 13,562(1968)].

[4] ROSENBLUTH, M.N., ROSS, D.W., KOSTOMAROV, D.P., Nucl. Fusion 12,3(1972).

[5] TANG, W.M., Nucl. Fusion 13,883(1974).

[6] GLADD, N.T., ROSS, D.W., Phys. Fluids 16,1706(1973).

[7] TANG, W.M., Phys. Fluids 17,1249(1974).

[8] DOBROWOLNY, M., ROSS, D.W., Phys. Fluids 18,717(1975).

[9] JABLON, C., Phys. Rev. Lett. 28,880(1972).

[10] LAQUEY, R.E., MAHAJAN, S.M., RUTHERFORD, P.H., TANG, W.M., Phys. Rev. Lett. 34,391(1975).

[11] Kadomtsev, B.B., Pogutse, O.P., in Reviews of Plasma Physics, edited by N. Leontovich (Consultants Bureau, New York, 1970) Vol. 5.

[12] Kadomtsev, B.B., Pogutse, O.P., Nucl. Fusion 11,67(1971).

[13] Ehst, D.A., Ph.D Thesis, Mass. Inst. of Tech., (1976).

[14] Horton, W., Ross, D.W., Tang, W.M., Berk, H.L., Frieman, E.A., LaQuey, R.E., Lovelace, R.V., Mahajan, S.M., Rosenbluth, M.N., Rutherford, P.H., Plasma Physics and Controlled Nuclear Fusion, Vol. 1 (IAEA: Vienna, 1975) p. 541. Lovelace, R.V., Tang, W.M., Bull. Am. Phys. Soc. 19,867(1974).

[15] Ott, E., Manheimer, W.M., Book, D.L., Boris, J.P., Phys. Fluids 16,855(1973); Manheimer, W.M., Ott, E., Chu, K.R., Boris, J.P., Callen, J.D., [to appear in Nucl. Fusion(1976)].

[16] Pogutse, O.P., Nucl. Fusion 9,157(1969).

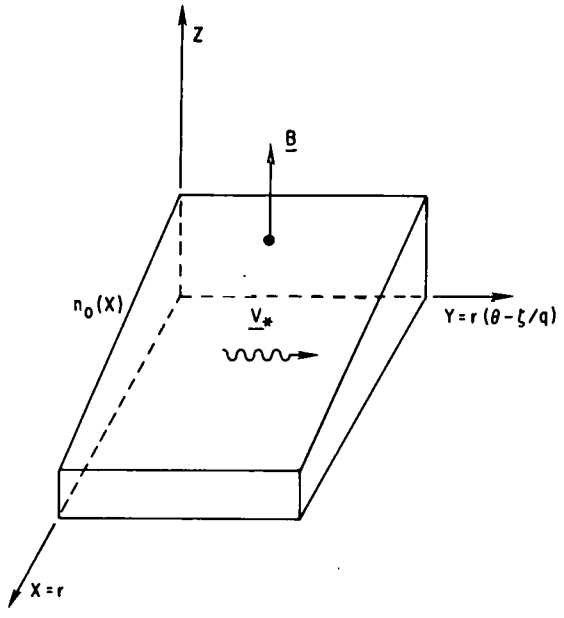

762110

Fig. 1. Relation of slab to toroidal coordinates showing mutually orthogonal density gradient $\nabla n_o(x)$, magnetic field B, and diamagnetic drift velocity V_* .

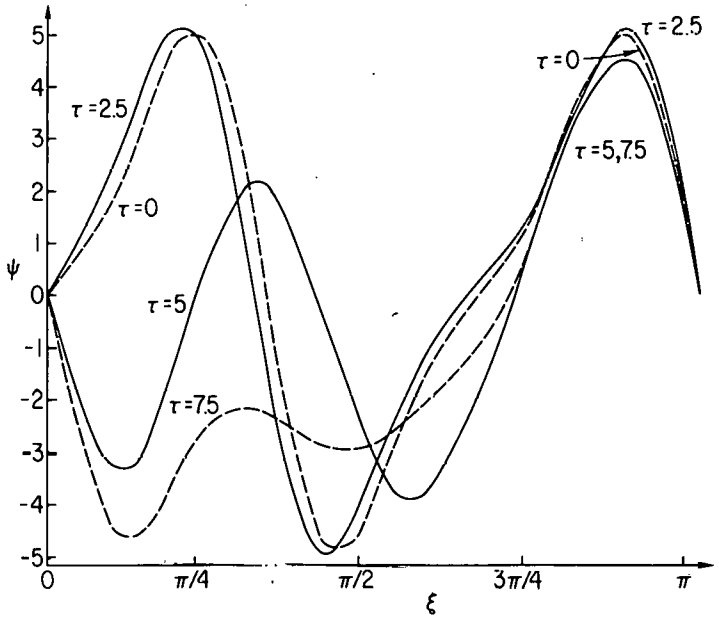

763177

Fig. 2. Time development (τ = 0.5, 2.5, 5.0, and 7.5) of a perturbed "two-mode" equilibrium: (p, 2p, 3p,...), p = 3; α = 0.05. There are 20 Fourier sine modes present. The equilibrium is linearly perturbed by modes m = 1 and 2, and is unstable to the formation of a steady configuration in which all the modes are excited.

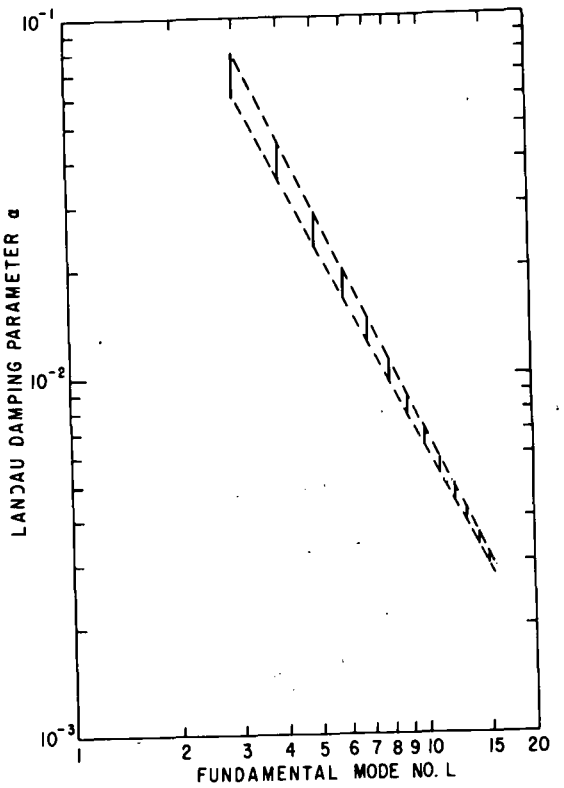

762058

Fig. 3. Stability windows for "two-mode" equilibria shown as vertical bars at fundamental mode numbers L for values of the relative Landau damping parameter α .

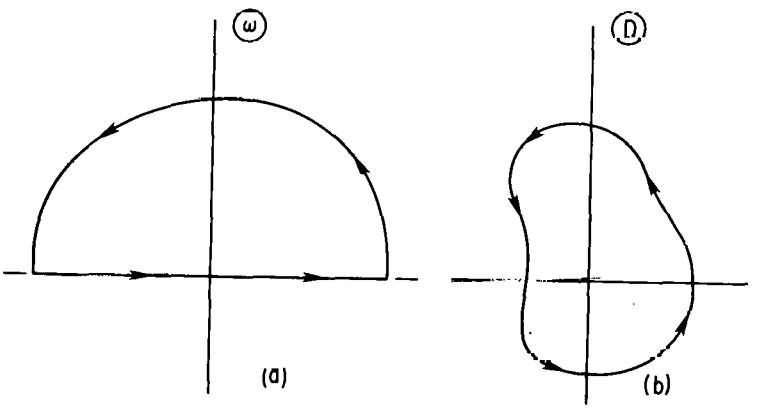

762108

Fig. 4(a). The usual Nyquist contour. (b) The topology of the Nyquist plot for m = 0.15 and radius of semicircle in (a) equal to 5. The plot encircles the origin once in the positive sense, indicating an unstable pole within the ω contour of (a).

762107

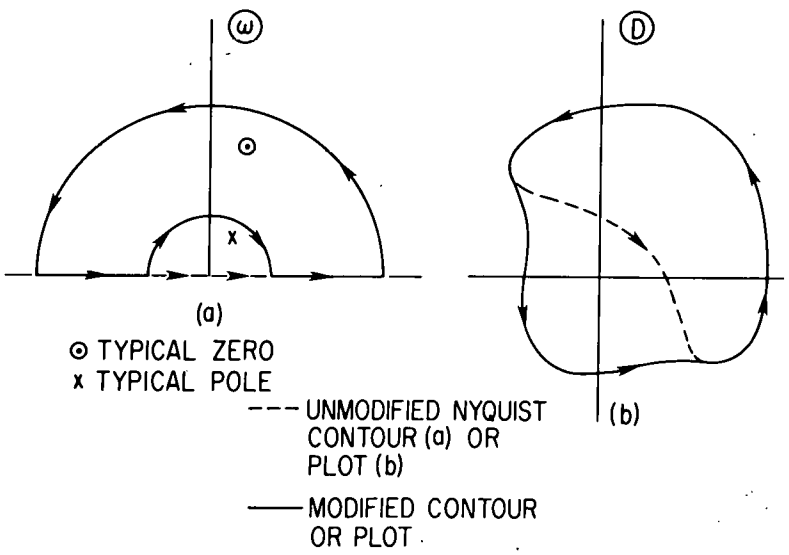

Fig. 59(a). The modified Nyquist ω contour necessary when the dispersion function has both zeros and poles. The locations of a typical zero and pole are indicated. (b) The topology of the Nyquist plot for m = 0.23 and the modified (indented) ω contour of (a). Instability is indicated. Also shown by the dashed line is the plot of the unmodified, semicircular ω contour. The D(ω) plot does not then encircle the origin, indicating an equal number of zeros and poles encircled by the ω contour.

763176

Fig. 6(a). Time development (τ = 0,5) of an m = 1, linearly perturbed coalesced "two-mode" and LMRT equilibrium (p,2p), p = 10 and α = 0.01; there are 25 Fourier sine modes present. A stable ($\alpha\ell^2$ = 0.64) "two-mode" equilibrium is generated (ℓ, 2ℓ,...), ℓ = 8. (b) Time development (τ = 0, 1.9, 2.0) of the same equilibrium, but linearly perturbed instead by the steady emission of low level noise. The asymptotic state is time-dependent or "bouncy" with average energy obeying the "two-mode" scaling.

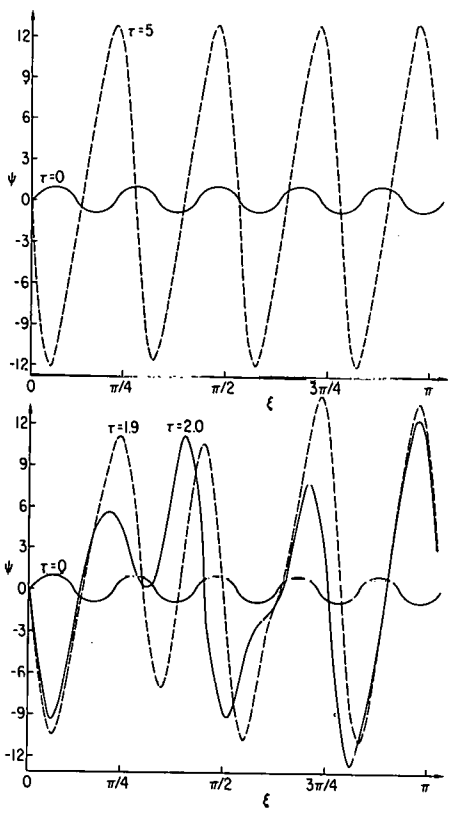

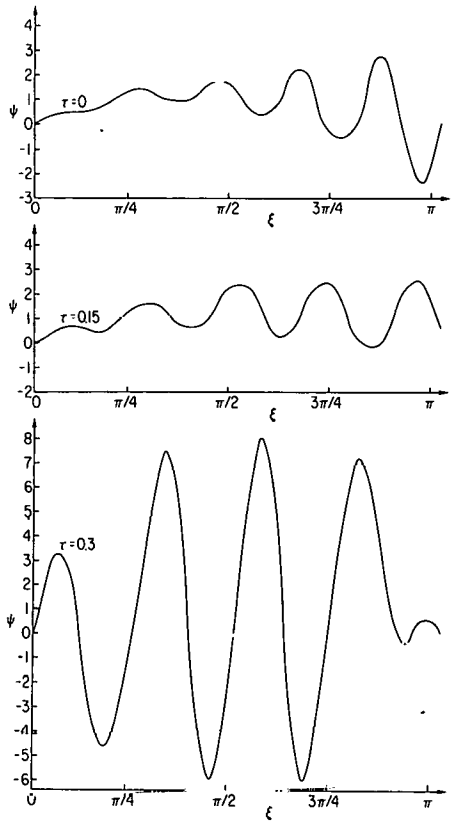

763175

Fig. 7. Time development (τ = 0, 0.1, 0.2, 0.3) of a linearly perturbed LMRT equilibrium
$\psi(\xi,o) = K\pi^{-1}\, nd(K\pi^{-1}\xi|k)\,[k^2 sn(K\pi^{-1}\xi|k)\,cn(K\pi^{-1}\xi|k)$
$+2(1-k^2)^{1/2}\sin(\alpha^{-1/2}\xi + \bar{\mu}\,\alpha^{1/2}\xi)] - (\alpha^{1/2}/3)\,[K\pi^{-1}(1-k^2)^{1/2}]^2\sin(2\alpha^{-1/2}\xi)$
where α = 0.01028, k = 0.9984, K(k) = 4.26, $\bar{\mu}$ = 1.39, and 36 Fourier sine modes were employed. This corresponds closely to the wave form shown in Fig. 1 of Ref. 10. The equilibrium is unstable and approaches the stable "two-mode" equilibrium in Fig. 6 for $\tau \geq 5$.

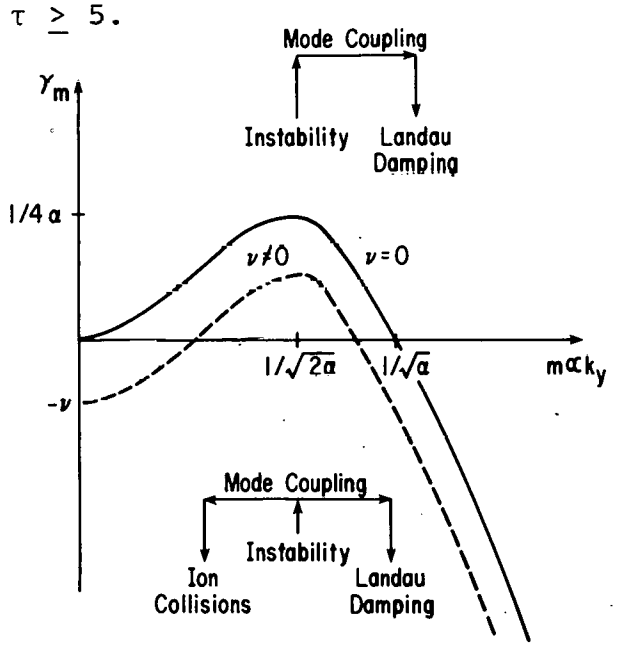

763179

Fig. 8. Diagram of the nondimensional linear growth rate $\gamma_m = m^2 - \alpha m^4 - \nu$ as function of mode number m($k_y = m/r$ with parameter $\nu \equiv \nu_+\nu_-/\omega_o^2$. The flow of wave energy is schematically presented.

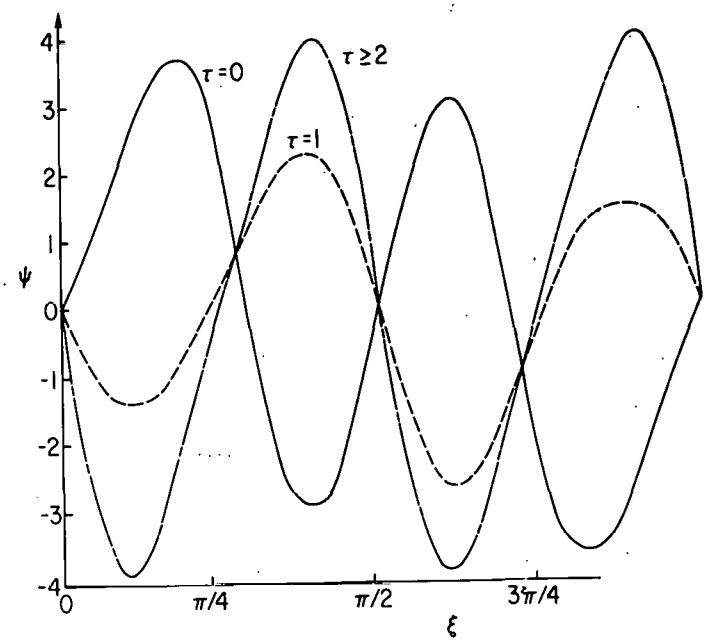

763178

Fig. 9. Time development (τ = 0., 1.0, 2.0) of an m = 8 perturbed three-mode equilibrium (p, 2p, 3p), with p = 2, α = 0.04, ν = 3.5, and 10 odd parity Fourier modes. The initial configuration is unstable to the formation of two-mode equilibrium (ℓ, 2ℓ), ℓ = 4.

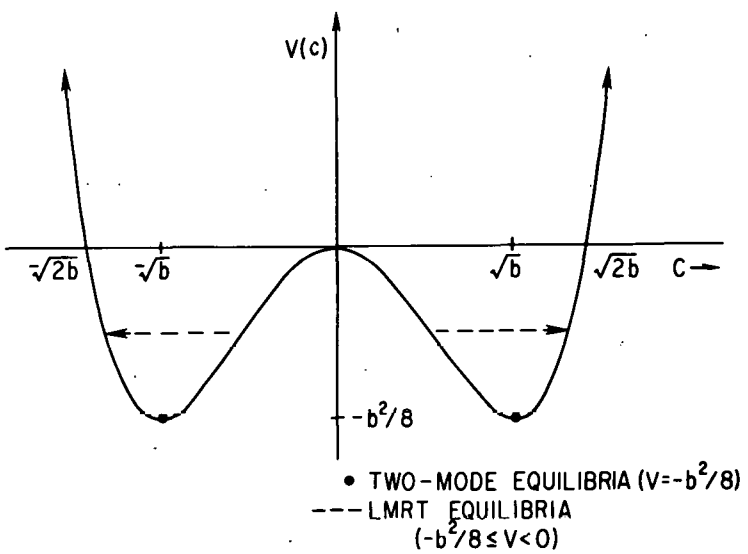

762111

Fig. 10. The classical potential well whose derivative is the second term of Eq.(3.2).

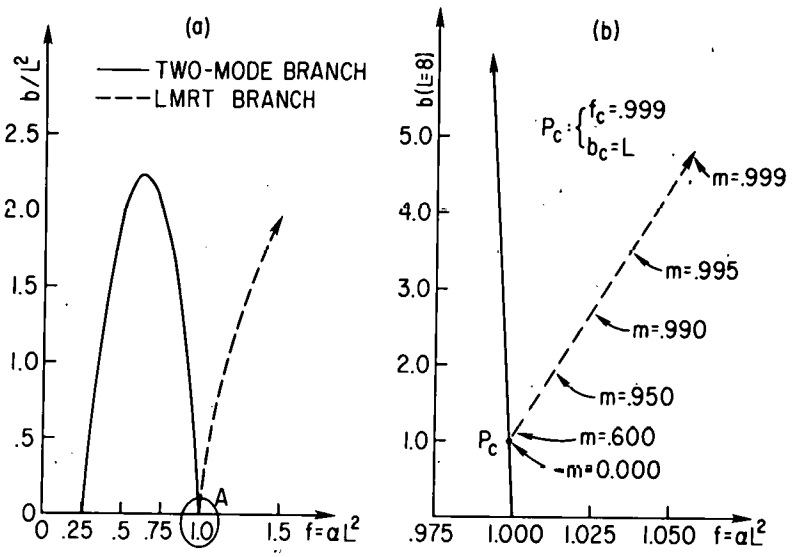

762130

Fig. 11(a). The branches of the nonlinear eigenvalue equation, Eq. (3.4). The orderings required for the LMRT branch are not valid outside of region A. (b) A blowup of region A in (a) for the fundamental mode number L = 8. The coalescence of the two-mode and LMRT branches is apparent.